1.The text should be close to final now. The figures should polished.

Atomistic resolution structure and dynamics of lipid bilayers in simulations and experiments

O. H. Samuli Ollila[1,*] and Georg Pabst[2]

[1]*Aalto University*

[2]*University of Graz, Institute of Molecular Biosciences, Biophysics Division, NAWI Graz, Humboldtstr. 50/III, Graz, Austria*[†]

(Dated: November 17, 2015)

Accurate details on the sampled atomistic resolution structures of lipid bilayers can be experimentally obtained by measuring C–H bond order parameters, spin relaxation rates and scattering form factors. These parameters can be also directly calculated from the classical atomistics resolution molecular dynamics simulations (MD) and compared to the experimentally achieved results. This comparison measures the simulation model quality respect to the reality, and if the quality is sufficient, the simulation model gives structural interpretation for the experimental data. Significant advance of MD models is the joint interpretation of different experiments with the same model. Here we focus on phosphatidylcholine lipid bilayers due to largest available datasets, in both experiments and simulations. We conclude that the acyl chain region structure and rotational dynamics is generally well described in simulation models, consequently the simulations can be considered as the state of the art model for the lipid bilayer hydrophopic region. Also changes with temperature, dehydration and cholesterol concentration are qualitatively correctly reproduced, however, the quality of atomistic resolution structural changes is not clear. In contrast, the lipid bilayer properties at the interfacial region, e.g. glycerol backbone and choline structures, and cation binding, are described less accurately in simulations. Thus extreme care must be taken when simulations are applied to understand phenomena where interafacial region play a significant role.

INTRODUCTION

Atomistic resolution structure and dynamics of lipid bilayers has been studied with wide range of techniques for many decades motivated mainly by their presence and important role in biological systems [1–6]. Lipid bilayers play direct or indirect role in several physiological and pathological molecular scale processes [7–9]. To fully understand these processes the atomistic and molecular level understanding of lipids is required. Since atomistic resolution studies are extremely difficult for biological membranes, simplified lipid-only systems are often used [1–6, 10]. The biological relevance of these model systems is supported, e.g. by similar NMR order parameters mesured from living cells, lipid extracts and model systems [2, 11, 12].

The most detailed information about lipid bilayer atomistic resolution structure and dynamics has been achieved with various Nuclear Magnetic Resonance (NMR) and scattering techiques [2–5, 10, 13–15]. The first one giving direct information on structures sampled by individual lipid molecules [2–4, 10] and the latter one giving complementary information on average bilayer properties, like e.g. area per lipid or bilayer thickness [5, 13–15]. Both techniques give robust, accurate and reproducible quantities related to the strucuture and dynamics. However, for structural and dynamical interpretation both techniques need to model experimental data to produce the measured quantities [2–5, 13–15].

On the other hand, remarkable progress in hardware and software allows to routinely perform classical atomistic resolution molecular dynamics (MD) simulations of lipid bilayer with duration of tens or hundreds nanoseconds. Ideally the molecules are sampling realistic conformations with realistic speed in these simulations. This can be verified by calculating directly measurable quantities from simulations and comparing these to experimental values. Here we review such comparisons for different experimental observables: C–H bond order parameters, spin relaxation times and form factor. The first and second parameters are measured with NMR. Hence, they represent to structure and dynamics sampled by individual lipid molecules, respectively. The third quantitiy is obtained from elastic X-ray or neutron scattering experiments and encodes the overall structural bilayer properties.

The order parameters and spin lattice relaxation times have been compared between simulations and experiments for validation and interpretation since the early days of lipid MD simulations [16, 17]. On the other hand, scattering form factors for lipid bilayers have been replacing the comparisons of simulations to the experimental area per molecule during the last decade since form factor is directly measurable quantity while area per molecule value depends on model used to analyze the scattering data [5].

If an atomistic resolution model reproduces all the above mentioned experimental parameters, i.e. order parameters, spin relaxation rates and form factor, the simulation can be considered as an ultimate model giving interpretation for all these experiments simulatenously. In addition, it would be the correct atomistic resolution representation of the system with high probability since it reproduces large amount of indepentedly measured experimental parameters simultaneously. Thus, usage of the model for further specific questions and applications would be well justified.

Here we discuss comparisons of order parameters, spin relaxation rates and scattering form factors between simulations and experiments in order to quantify the simulation model quality and interpret the experiments. Also related technical details on experimental data and simulation analysis are dis-

cussed. We focus on phosphatidylcholine lipid bilayers due to most comprehensive available datasets for both, simulations and experiments. However, the basic ideas of the approach is valid also for other molecules [18–20]. We pay special attention on the accuracy and applications of the NMR order parameter data for the glycerol backbone and choline which is often overlooked in the literature. Changes in lipid bilayer properties with varying conditions and the relation to, e.g. ion partition are also discussed.

The general conclusion is that the hydrophopic acyl chain region is well described in simulation models, thus the simulations can considered as the state of the art model with atomistic resolution for this region. However, the glycerol backbone and choline regions are less well described in simulation models, thus extreme care must be taken when phenomena related to the interfacial region are studied with simulations. Due to the large variation of lipid headgroups present in biological systems, the chemical and structural details of the interfacial region are expected to be relevant in several biochemical processes. For example, cell membrane interactions with ions, drug molecules and proteins may be regulated by these details. Here we demonstrate how atomistic resolution model quality can be estimated to minimize the artificial conclusions produced by simulations.

C-H BOND ORDER PARAMETERS AS ATOMISTIC RESOLUTION STRUCTURAL MEASURE

Definition and properties of C-H bond order parameter

In lipid bilayer systems the order parameter of a hydrocarbon C–H vector is typically defined as

$$S_{\mathrm{CH}} = \frac{1}{2}\langle 3\cos^2\theta - 1\rangle, \qquad (1)$$

where the angle brackets denote an ensemble average over the sampled conformations, and θ is the angle between the C–H bond and the membrane normal. The numerical values of order parameters vary between $-\frac{1}{2} < S_{\mathrm{CH}} < +1$ depending on the sampled θ distribution. The definition is motivated by its connection to the dipolar and quadrupolar splitting measured with ^{1}H-^{13}C NMR and ^{2}H NMR techniques, respectively. The functional form comes from the fundamental theory of interactions between spin systems which gives a connection between average molecules orientations and NMR measurables [21].

If the sampled distribution of θ for a C–H bond are known, the order parameter can be straighfowardly calculated from Eq. 1. However, the sampled θ distribtions cannot be uniquely determined from the known order parameter. Thus the experimental order parameter values gives a set of conditions which the structural molecular model (more specifically the C–H bond vectors of the model) has to fulfill, but the experimental order parameters alone cannot be used to uniquely resolve the structure. The same applies practically to all experimental parameters used in biomolecular structure determination.

Atomistic resolution molecular dynamic simulations naturally produces the sampled structures and the calculated θ distributions can be substituted into Eq. 1 to calculate the order parameters. If and only if the experimental order parameters are reproduced, the sampled structures can be considered as a realistic atomistic resolution representation and used to interpretate experimental order parameters. Before MD simulations were feasible for such usage, other models have been used for this interpretation [22–29]. It is important to note, however, that reproduction of the order parameters does not absolutely guarantee that the sampled structures are correct since several structural models can produce the same order parameters, in principle. Significant advance of the MD models compared to the traditional models is that the same MD structures can be straightforwardly compared to other experimental observables in addition to order parameters, like ^{31}P chemical shift anisotropy [30], ^{31}P-^{13}C dipolar couplings [31], spin relaxation data [32] and scattering data [33]. The comparisons of the same model to the various independently measured experimental observables significantly reduces the possibility of getting unrealistic structures.

The probability for unrealistic structures is further reduced by the large amount of experimentally available order parameter values. As discussed in this review, the order parameters can be measured with high accuracy for each C–H pair of a lipid molecule in a liquid crystalline bilayer [2, 3, 10, 34–37]. Also the signs [28, 34, 38] and stereospecifity of C–H segments in the same carbon (*forking*) [11, 34–36, 39, 40] are experimentally available. Consequently, a realistic atomistic resolution model, for example, for POPC molecule (see Fig. 1 B)) in liquid crystalline bilayer has to reproduce 82 experimental order parameter values. If these parameters are not reproduced for certain segments, the model deficiencies are easy to localize since the segmental order parameter is a very local quantity depending only on the position of two atoms (C-H pair). This is an advance over several other accurately measured NMR quantities depending on the position of several atoms [30, 31], thus complicating the localization of structural differences in the case of disagreement between model and experiments.

Experimental order parameter data for single component lipid bilayers are easily available in the literature [36, 37, 57–62]. The amount of data, especially from ^{13}C NMR, has been also increasing of late [36, 57, 58, 61, 62]. Further, changes of order parameters for all lipid segments have been measured various experimental different conditions, like temperature [22–24, 63], hydration level [35, 43, 64, 65] and in the presense of ions, charged objects [42, 66–68], cholesterol [36, 62, 63, 69] and proteins [61, 70, 71]. Since the comparison of order parameter responses between experiments and simulations has not been much utilized, we will exemplify its potential by showing the effect of Na^+ ions on choline order parameters and its relation to ion partition in simulations [72] and experiments [42, 66–68].

In this work we discuss only order parameters obtained

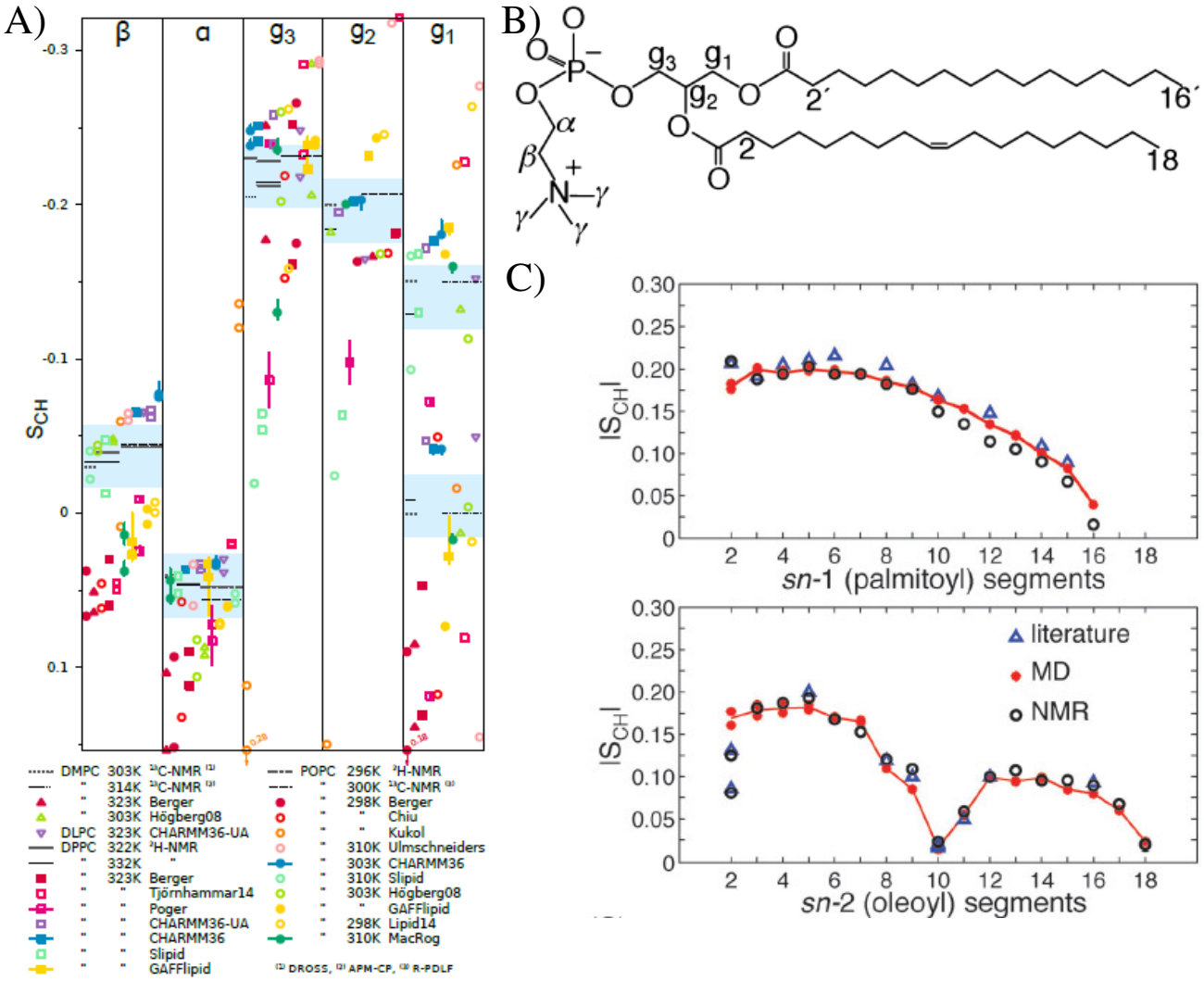

FIG. 1: A) Order parameters from simulations and experimens for phosphatidylcholine headgroup and glycerol backbone segments adapted from Botan et al. [37]. The blue shaded regions show the subjective sweetspots where the simulation data should fall to agree with experiments, based on estimated quantitative accuracy of order parameter measurements by Botan et al. B) Chemical structure of 1-palmitoyl-2-oleoylphosphatidylcholine (POPC). C) Order parameters $|S_{\mathrm{CH}}|$ for POPC acyl chains from ^{1}H-^{13}C NMR at 300K (black dots) [36], from ^{2}H NMR at 300K (blue triangles, literature) [25, 41] and from MD simulations at 298K (red dots) [36]. The experimental values shown in A): DMPC 303 K [34], DMPC 314 K [35], DPPC 322 K [23], DPPC 323 K [42], POPC 296 K [43], and POPC 300 K [36]. The force fields in A): Berger [44], Hogberg08 [45], Poger [46], Ulmschneiders [47], Kukol [48], Chiu [49], CHARMM36 [50], GAFFlipid [51], Slipid [52], MacRog [53], Tjörnhammar14 [54], Lipid14 [55], CHARMM36-UA [56]. The interactive version of A) is available at https://plot.ly/∼HubertSantuz/72/lipid-force-field-comparison/.

from multilamellar samples, as they are the closest experimental analogue to MD simulations with periodic boundary conditions. We do not discuss order parameters measured for other type of samples, such as bicelles [73–75], or indirect measurements by using, e.g. relaxation data [76] since the comparison to the standard simulation setup is less straightforward.

Order parameters from ^{2}H NMR experiments

The absolute values of order parameters are connected to the quadrupolar splitting $\Delta\nu_Q$ in ^{2}H NMR experiments through the equation

$$|S_{\mathrm{CD}}| = \frac{4}{3}\frac{h}{e^2 qQ}\Delta\nu_{\mathrm{Q}}, \tag{2}$$

where e is the elementary charge, Q is the deuteron quadrupole moment and h is the Planck's constant. The parameter q is related to the largest electric field gradient

and in practise its value is not known; therefore the static quadrupolar coupling constant $\frac{e^2qQ}{h}$ is defined, and its is value measured for different compounds in their solid state ($\Delta\nu_Q$ measurement from the system where order parameter is known to be 1). The value measured for different alkenes, $\frac{e^2qQ}{h}$=170 kHz is typically used in C-D order parameter measurements for lipids. The relation between order parameters and quadrupolar splittings then becomes $S_{\mathrm{CD}} = 0.00784 \times \Delta\nu_{\mathrm{Q}}$. With this relation the quadrupolar splittings reported in the literature can be translated to the order parameter values. For a review and more accurate description see, e.g. Ref. [10].

For ^2H NMR measurements the CH_2 segments have to be labeled with deuterium. This can be done specifically for a certain segment or for the several segments simultaneously [3, 4, 59]. In the first case, it is known that the measured order parameter (quadrupolar splitting) is related to the labeled segment. In the latter case several order parameters (quadrupolar splittings) are measured which arise from all the labeled segments, however, it is not known which order parameter belongs to which CH_2 segment. Majority of the ^2H NMR data in the literature are measured using samples with perdeuterated acyl chains [59, 60] while also order parameter data from specifically deuterated lipids are available for several lipid types in various conditions [11, 22, 24, 25, 39, 42, 63, 64, 66, 68, 70, 71].

Order parameters from ^{13}C NMR experiments

The order parameter can be related to the dipolar splitting $\Delta\nu_{\mathrm{CH}}$ from ^{13}C-^{1}H NMR experiment which is related to the effective dipolar coupling d_{CH} through a scaling factor depending on the used pulse sequence [34–36, 38]. The effective dipolar coupling d_{CH} is then connected to the absolute value of order parameter through equation

$$|S_{\mathrm{CH}}| = (\frac{D_{\mathrm{max}}}{2\pi})^{-1} d_{\mathrm{CH}}, \quad (3)$$

where $D_{\mathrm{max}} = \frac{\hbar\mu_0\gamma_h\gamma_c}{4\pi\langle r_{\mathrm{CH}}^3\rangle}$. r_{CH} is the C-H distance, μ_0 is the vacuum permittivity, and γ_h and γ_c are the gyromagnetic constants for ^{1}H and ^{13}C nuclei. In contrast to Eq. 2, all the parameters in Eq. 3 are in principle known. However, for the internuclear distance only the average $\langle r_{\mathrm{CH}}\rangle$ is known, but not the third moment $\langle r_{\mathrm{CH}}^3\rangle$. For this reason frequencies between 20.2-22.7 kHz have been used for $\frac{D_{\mathrm{max}}}{2\pi}$ [32, 34–36, 38, 77].

In contrast, specific labeling is not needed for ^{13}C NMR experiments due the natural abundance of ^{13}C. Labeling can be, however, used to enhance the signal for a specific segment of interest [78]. Order parameter measurements with ^{13}C NMR are 2D experiments, the chemical shift being in the first dimension and dipolar coupling in the second [34–36, 38]. The chemical shift depends on the local chemical environment and is different for each carbon segment. In the second dimension the dipolar coupling (order parameter) corresponding to each chemical shift value is measured, and its value can be connected, in principle, to each carbon segment by using the chemical shift value. This is straighforward for hydrocarbon segments in choline, glycerol backbone, close to the double bonds, and in the beginning and the end of acyl chains due to their distinct chemical shift values [34–36, 38, 62]. Challenges occur in the acyl chain region, where chemical shift values of different segments are very close to each other [34–36, 38, 62]. This issue has been solved by filtering the spectra by using partially deuterated lipids and data from simulations to help the assigment [36, 62].

Quantitative accuracy of experimental order parameter values

It must be stressed that ^{2}H NMR and ^{13}C NMR are fully independent experiments since the deuterium quadrupolar splitting $\Delta\nu_Q$ and the dipolar splitting d_{CH} are different physical observables. In addition, the prefactors connecting the observables to the order parameter (Eqs. 2 and 3) are independently measured. Further independent experiments are performed by measuring the ^{1}H-^{13}C dipolar couplings using different pulse sequences [34–36, 38] when the connection between dipolar splitting $\Delta\nu_{\mathrm{CH}}$ and effective dipolar coupling d_{CH} is different.

The measurements of quadrupole $\Delta\nu_Q$ and dipolar d_{CH} splittings are relatively accurate, especially for quadrupolar splitting. **2.How accurate exactly?** Thus the quantitative accuracy of measured order parameters is determined in practise by the prefactors connecting the splittings and order parameters in Eqs. 2 and 3. Since the prefactors are determined independently in ^{2}H and ^{13}C NMR measurements, the quantitative accuracy is best estimated by comparing the measured order parameter values from different experiments.

These comparisons are done by several authors and generally show a very good agreement [34–37, 62]. Botan et al. collected literature values for PC lipid choline headgroup and glycerol backbone order parameters and suggested that order parameters are known with the accuracy of $\pm$0.02 for these segments in purified PC lipid bilayer samples [37] which agrees with the estimate of Gross et al [34]. Based on this estimation Botan et al. suggested sweet spots where choline and glycerol backbone order parameters from simulations should range, see Fig. 1 A). Also acyl chain order parameters from different techniques are in good agreement when compared by several authors [34–36, 62], however the 0.02 accuracy might not be achieved for some segments.**3.Maybe specify to which ones?.** The comparison by Ferreira et al. [36] for POPC acyl chains is also shown in Fig. 1 C).

Qualitative accuracy of experimental order parameter values

When order parameter changes are measured with varying conditions, like temperature [22, 24, 63], hydration

level [35, 43, 64, 65], presense of ions [42, 66–68], cholesterol [36, 62, 63, 69] or proteins [61, 70, 71], the prefactors connecting order parameters and measured couplings in Eqs. 2 and 3 can be considered to be unchanged. Therefore, accuracy of the measured change is determined by the accuracy of the splitting measurement, in contrast to the quantitative accuracy discussed in previous section. Here we refer to this as a qualitative accuracy. Due to the high resolution of splitting measurements, especially in ^{2}H NMR, the qualitative accuracy is much higher than the quantitative accuracy.

The high qualitative accuracy of order parameter measurements is demonstrated in Figs. 2 and 3 showing the measured changes as a function of ion concetrations and hydration level, respectively. Systematically observed order parameter decrease of choline α and β segments due to penetrating positive charges [42, 66–68] from ^{2}H NMR are shown in Fig. 2 A). The quadrupole splittings reported in the original work [42] and corresponding order parameters are shown. The distinct quadrupolar splitting changes correspond to order parameter changes below 0.03 and 0.05 units for β and α, respectively. Systematically observed increase for choline β and α segments due to decreased hydration level are shown in Fig. 3. A similar increase is observed for different phosphatidycholine lipids in slightly different temperatures by different groups using both ^{2}H NMR [43, 64] and ^{13}C NMR [79]. The results demonstrate the systematic changes only slightly above 0.01 units can be detected also with ^{13}C NMR [79].

In conclusion, the order parameter changes can be measured with very high accuracy, thus even very small structural changes can be observed. Molecular models are necessary to analyze the measured changes to avoid overinterpretation of minute changes observed in experiments. For example, high concentration of cholesterol induces measurable changes (less than 2 kHz) to the DPPC α and β quadrupolar splittings, however, the related structural changes are probably almost negligible [37, 69].

Signs of order parameters

^{2}H NMR [10] and standard ^{1}H-^{13}C NMR [34–36, 38] measure only the absolute value of order parameter. However, two different ^{1}H-^{13}C NMR techniques applied to eggPC [38] and DMPC [34, 38] allow also the measurement of the sign. The experiments report negative order parameters for almost all the segments, only α and γ are positive. Furthermore, the signs [28, 34, 38] and magnitudes [11, 36, 37] of choline headgroup and glycerol backbone order parameters are practically unaffected by the acyl chain contents of the bilayers. The results indicate that the order parameter signs for these segments can be assumed to be the same in all PC lipids in bilayer. On the other hand, positive signs for g_1, g_3 and C_2 have been reported by Aussenac et al. [73], which has led to some confusion in the simulation community [45, 80, 81]. However, these signs were not directly measured but extracted from the model used to interpret ^{2}H NMR order parameters from DMPC bicelles [73]. Thus, it is reasonable to conclude that order parameters are negative for all segments except for α and γ, as directly measured with ^{1}H-^{13}C NMR [28, 34, 38].

In measurements of order parameter changes with respect to varying conditions [22, 24, 35, 36, 42, 43, 61–71] only the absolute values are measured. However, the experiments are usually done by gradually changing the conditions and systematic order parameter responses are observed [36, 42, 43, 64–66, 79] (see also Figs. 2 and 3), indicating that sudden changes of sign do not occur. On the other hand, the large amount of bound positive charge may decrease the α carbon order parameter below zero as demonstrated by the spectra measured by Altenbach and Seelig [66] for POPC with high concetrations of $CaCl_2$, shown in Fig. 4.

Forking of order parameters

The order parameters for two C–H bonds in the same CH_2 segment are equal for the most lipid segments [11, 22, 24, 25, 34–36]. Exceptions in a fluid PC lipid bilayer are g_1, g_3, and the C_2 carbon in the *sn*-2 chain segments as observed with both ^{2}H NMR [11, 25, 39, 40] and ^{1}H-^{13}C NMR techniques [34–36], see also Fig. 1. We call this phenomena *forking*, as done also previously to avoid confusion with splittings measured with NMR [37].

The forking has been studied in detail with ^{2}H NMR techniques by separately deuterating the R or S positions in CH_2 segments in order to assign order parameters to correct hydrogens [11, 40]. These studies also show that the forking arises from differently sampled orientations of the two C–H bonds, not from two separate populations of lipid conformations [11, 40]. This means that realistic atomistic resolution molecular model has to reproduce the forking correctly and that the isomeric positions of hydrogens must be taken into account when calculating order parameters from simulations [37].

Order parameters from simulations

Since all the atom coordinates are available from a molecular dynamics simulation trajectory, the order parameters can be calculated directly from the definition in Eq. 1. The ensemble average is taken over the simulation time and all the molecules in simulation. The hydrogen positions can be generated post-simulationally based on heavy atoms positions and the known hydrocarbon geometries for united atom simulations without explicit hydrogens by creating a trajectory with added hydrogens [37, 82] or by using equations to directly calculate order parameters [83, 84]. The first approach is appropriate for accurate structural studies since it allows to analyse forking in contrast to the latter technique.

The difference in the analysis methods for the forked segments is most likely the reason for diverging choline and glycerol backbone order parameters reported for the same models

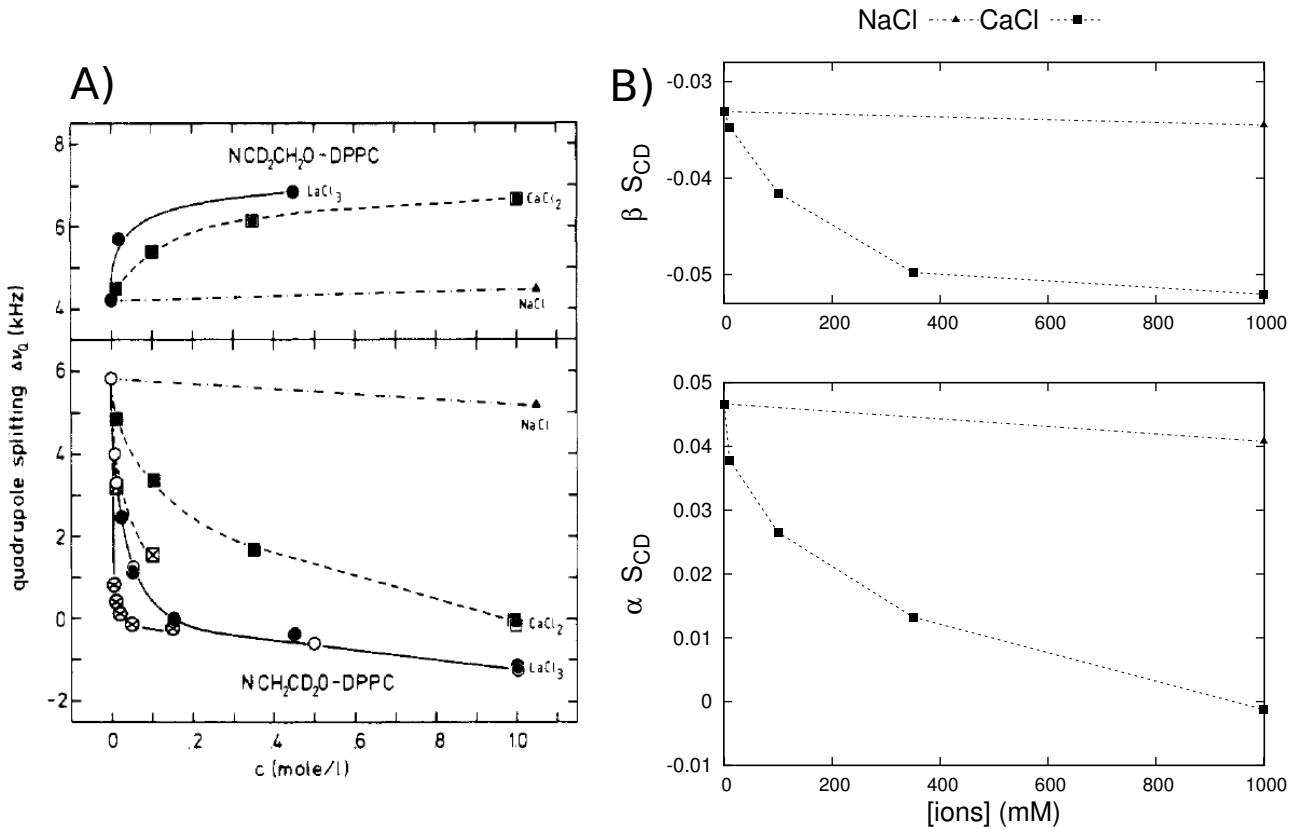

FIG. 2: A) Quadrupolar splittings of DPPC α and β segments as a function of different ion concetrations measured by Akutsu and Seelig with ^{2}H NMR [42]. B) The measured quadrupolar splittings with NaCl and $CaCl_2$ translated to order parameters ($S_{\rm CD} = 0.00784 \times \Delta\nu_{\rm Q}$). The negative sign for β order parameter is assigned according to more recent experiments [28, 34, 38] (see also Ref. [37] and Section 3). These changes were later shown to be consistent with the addition of different charges into the bilayer, and the electrometer concept was introduced to measure the amount of charge incorporated in the bilayer interface [42, 66–68].

by different authors [37, 85]. Also different order parameters for C–H segments attached to double bond are reported for the same model [82, 86] due to a bug in a widely-used version of the *g_order* program in the Gromacs package. The *g_order* program also prints -$S_{\rm CH}$, which is the most likely reason for the reported positive order parameters for acyl chains in some studies [87]. When these technical issues are taken into account, the different order parameters calculations from simulations are in good agreement.

The statistical error for order parameters is estimated by using the error of the mean for time blocks [82], independent simulations [85] and different lipids [37]. All these approaches yield a maximum error of $\sim \pm 0.01$.

It was recently pointed out that the sampling of individual dihedral angles might be very slow compared to the typical (100 ns) simulation timescales [88]. This result raises a question if the molecules sample the full phase phase during typical simulation time scales. On the other, another recent study showed that the slowest rotational auto-correlation function observed (for g_1 segment) in the Berger model reached a plateau ($S^2_{\rm CH}$) after $\sim$200 ns and its relaxation was significantly too slow compared to NMR relaxation experiments [32], see Fig 8. This indicates that the typical simulation times are long enough for full conformational phase space sampling for the models with realistic dynamics [32].

Comparison between order parameters from simulations and experiments

The acyl chain order parameters are compared between simulations and experiments since the early days of lipid bilayer simulations [16, 44, 83, 89–98]. Good agreement has been generally found [30, 44–56]. except for the C_2 segment of the *sn-2* chain having low magnitude and significant forking in all PC lipids, in constrast to C_2 of the chain linked to *sn*-1 [22, 34–36, 39], for example see Fig. 1 C). This feature is, however, not analyzed or not reproduced for several lipid models [30, 45, 47–49, 51–54, 99]. Some models report the small order parameter for C_2, but the forking is not correctly reproduced or analyzed [30, 50, 55, 99]. Among all studied force fields, the united atom CHARMM36 is closest to the experimental results [56].

Also acyl chain order parameter changes with varying conditions are compared between simulations and experiments by several authors. Experimentally observed order parame-

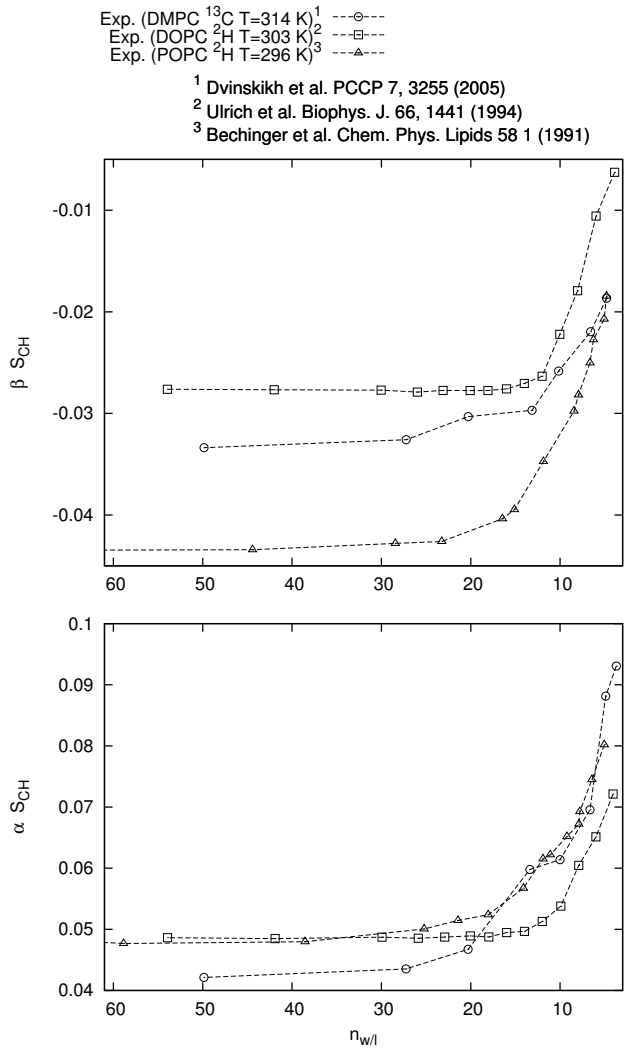

FIG. 3: Systematic increase of phosphatidylcholine α and β order parameters with decreasing hydration level, observed with both ^{2}H NMR [43, 64] and ^{13}C NMR [79]. The negative sign for β order parameter is assigned according to more recent experiments [28, 34, 38] (see also Ref. [37] and Section 3). The choline order parameter increase is related to the P-N vector tilting more parallel to the membrane plane [37] while relation between order parameter decrease and tilting more perpendicular has been suggested [68].

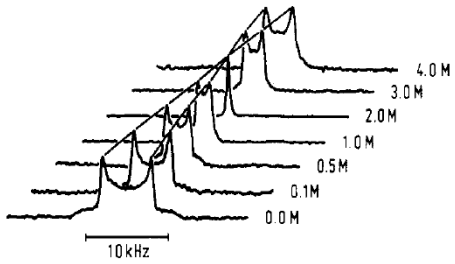

FIGURE 1: ^{2}H NMR spectra of coarse dispersions of POPC bilayers at various $CaCl_2$ concentrations (no NaCl). The lipid was deuterated at the α-segment ($-NCH_2CD_2OP-$). Measuring temperature, 40 °C.

FIG. 4: Quadrupolar splitting $\Delta\nu_Q$ for α segment in POPC as a function of $CaCl_2$ concentration measured by Altenbach and Seelig [66]. The splitting is related to the order parameter as $S_{\rm CD} = 0.00784 \times \Delta\nu_Q$. More recent studies show that the α order parameter is positive in the absense of $CaCl_2$ [28, 34, 38]. Thus, the most obvious interpertation is that the α order parameter decreases to zero when $CaCl_2$ concentration reaches 2.0M, and becomes increasingly negative with further addition of $CaCl_2$. Reprinted with permission from Altenbach and Seelig, Biochemistry, 23, 3913 (1984). Copyright 1984 American Chemical Society.

ter increase with cholesterol concentration [36, 63, 84, 100–102] and dehydration [65, 79] is observed also in simulations [36, 80, 84, 103–107], as well as the temperature induced order parameter decrease [63, 108]. A more careful comparison reveals, however, that the temperature and dehydration effects are slightly underestimated in simulations compared to experiments [80, 108]. Also cholesterol effects to DMPC bilayer are underestimated in the CHARMM36 model [105], while Slipids [106] and Amber Lipid14 [107] models show satisfactory agreement. The comparison of a Berger/Höltje [44, 109] based model to the extensive data set with various POPC/cholesterol mixtures shows good agreement with experiments for low cholesterol concetrations, however, the agreement gets worse for cholesterol concentration $\geq$ 34% [36]. A recent comparison of the Amber Lipid14 model to the same experimental data shows signifincantly better agreement [107], shown in Fig. 5. The orientation of cholesterol ring structure is reasonable in all models [36, 84, 105, 107], however, the cholesterol acyl chain exhibits too low order parameters in the Berger/Höltje [44, 109] based model [36] and too much forking in Amber Lipid14 [107], while CHARMM36 reproduces experiments well [105].

The dip of the acyl chain order parameter profile due to double bonds is generally reproduced by different simulation models [36, 50, 51, 55, 56, 82, 86, 106, 110–118]. The particularly good agreement, often achieved for the oleyl chain in POPC bilayer with one *cis* double bond, is demonstrated in Fig. 1 C). Also the further order parameter decrease due to multiple double bonds (polyunsaturation) [82, 86, 110, 111, 113–115, 117, 118] is usually well reproduced, as demonstrated in Fig. 6 for Berger [44] based model with double bond description by Bachar et al. [86]. Also difference between *cis* and *trans* double bonds can be reproduced in MD simulations [119].

In contrast to acyl chains, the glycerol backbone and choline order parameters are not routinely compared between simulations and experiments. In most comparisons the experimentally available signs, stereospecific labeling and high accuracy are not fully exploited [18, 37, 45, 50, 51, 80, 85, 97]. These issues were recently dicussed by Botan et al. who also compared order parameters between 13 different simulation models and experiments [37]. The results, shown also

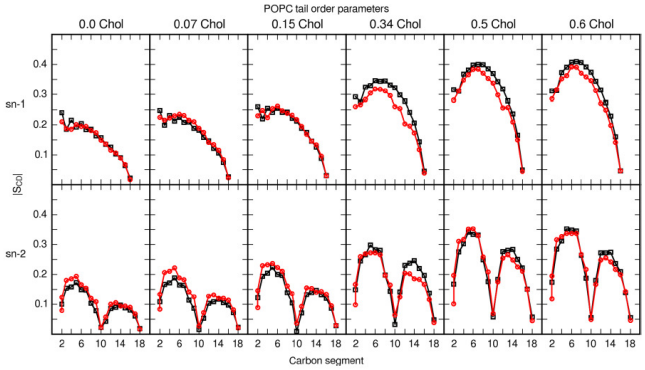

FIG. 5: Cholesterol effect on acyl chain order parameters compared between ? model [107] and experiments [36]. The agreement with experiments with this model is significanly better than Beger/Höltje based model compared by Ferreira et al. [36].

in Fig. 1 A), reveal significant differences between models and experiments, and none of the available models reproduces all order parameters within experimental error. On the other hand, experimentally observed choline order parameter increase with dehydration [43, 64, 79] and decrease due to cation penetration [42, 66] were reproduced in simulations [37, 72]. However, especially the effect induced by Na^+ ion penetration is strongly overestimated in several models which arises most likely from an artificially high partition coefficient [72], as also demonstrated in Fig. 7. The effect of cholesterol on glycerol backbone and choline is overestimated by the Berger/Höltje based [36] and Amber Lipid14 [107] models while CHARMM36 and MacRog performed better [37].

In conclusion, the acyl chain order parameters and their qualitative changes are generally well described in atomistic MD models, except for C_2 segment in *sn*-2. However, all models have difficulties with varying severity to correctly describe the glycerol backbone and choline order parameters.

Interplay between simulations and NMR order parameters: Validation and interpretation

Since the acyl chain order parameters from MD models generally agree with experiments for single component lipid bilayers in full hydration, the conformations sampled in simulations can be considered as realistic atomistic resolution structures for the acyl chains (except for the C_2 segment in the *sn*-2 chain). As also the acyl chain rotational dynamics has the correct order of magnitude (see Section 3), the dynamical nature of hydrophopic region of lipid bilayers seen in simulation videos can be considered as a realistic representation of the system. This is significant advancement to the traditional static structural models [22, 25, 27, 122]. Since lipid bilayers are considered as a simple models for cell- and other biological membranes, the intuitive understanding of their dynamical nature has a significant impact on biomembrane physics and chemistry.

Also more detailed structural interpretation has been succesfull for acyl chain region, especially for order parameter decrease due to *cis* double bonds [82, 86, 114, 115, 123–125]. From NMR experiments alone it was not possible to judge if the order parameter decrease arises from the reduced chain order or the changes in average θ angle in Eq. 1 [124, 125]. The interpretation of NMR experiments with the help of MD simulations revealed that double bonds, indeed, decrease the chain order due to the flexible dihedral potentials next to the rigid double bonds [82, 86, 114, 115, 123–125].

The acyl chain order parameter increase and related bilayer thickening with cholesterol concentration [36, 84, 104–107], dehydration [80, 103] and reduced temperature [108] are qualitatively reproduced by simulations giving intuitive visualizations for these effects. However, the order parameter changes are often under- or overestimated [36, 80, 105, 108], thus it is not clear how well the models can be used for atomistic resolution intepretation of these changes. For example, delicate lipid-cholesterol interactions are known to induce liquid-ordereded and liquid-disordered phase coexistence [126]. To give atomistic resolution interpretation for this phenomena [127–130], the atomistic resolution structures and interactions should be correct, which does not seem to the case for several models [36, 105, 107].

Simulation studies have also predicted changes in the acyl chain region which are yet to be experimentally confirmed, e.g. order parameter decrease due to lipid oxidation and changes in order parameter sign in oxidized acyl chain [87].

The usability of MD models for structural interpretation decrease closer to the interfacial region since the experimental glycerol backbone, choline headgroup and *sn*-2 C_2 segment order parameters are not usually reproduced within experimental error, as discussed in the previous section. The forking and low order parameter values for C_2 in the *sn*-2 are related to the parallel orientation of the chain respect to membrane normal [39, 122] which is suggested to have significant contribution e.g. to membrane electrostatic potential [131]. Also the atomistic resolution structures sampled by glycerol backbone and choline headgroup are not

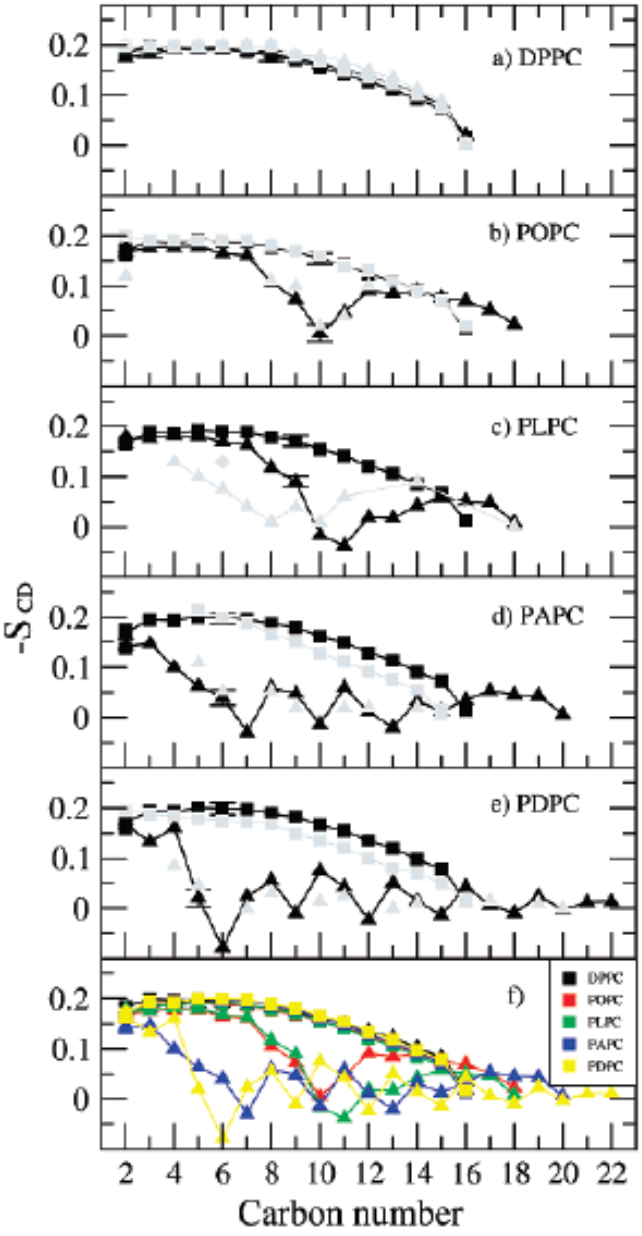

FIG. 6: Figure comparing order parameters in polyunsaturated acyl chains between simulations and experiments adapted from [82]. Order parameters for the sn-1 (squares) and sn-2 (triangles) chains of (A) DPPC, (B) POPC, (C) PLPC, (D) PAPC, and (E) PDPC. Simulation results are shown in full black, and experimental results for comparison in gray. Additionally, part F summarizes the data for all bilayers from the simulations. Experimental order parameters were chosen for comparison as follows. The order parameters for DPPC (T=323K) are based on studies by Petrache et al. [120] whereas the experimental S_{CD} values for PDPC and for the sn-1 chain of POPC (T=310 K) are based on studies by Huber et al. [114] For the sn-1 chain of PDPC, the data set at 310 K is obtained by linearly interpolating between data at 303 and 323 K, whereas for the sn-2 chain the data at 303 K are presented [114]. Experimental values for the sn-2 chain of POPC are based on studies by Seelig et al. [25] A single experimental value is available also for the sn-2 chain of the PLPC bilayer at 313 K (diamond) [27] to compare with our simulated order parameters for PLPC. Together with PLPC, there are also experimental results for PiLPC (T=313K) [27]. Experimental order parameters for the sn-1 and sn-2 chains of PAPC (T=303 K) are based on quadrupole splittings measured by Rajamoorthi et al. [121]. For the sn-1 chain the monotonic decrease through the acyl chain is expected. For the sn-2 chain, values are fitted such that the agreement is as good as possible.

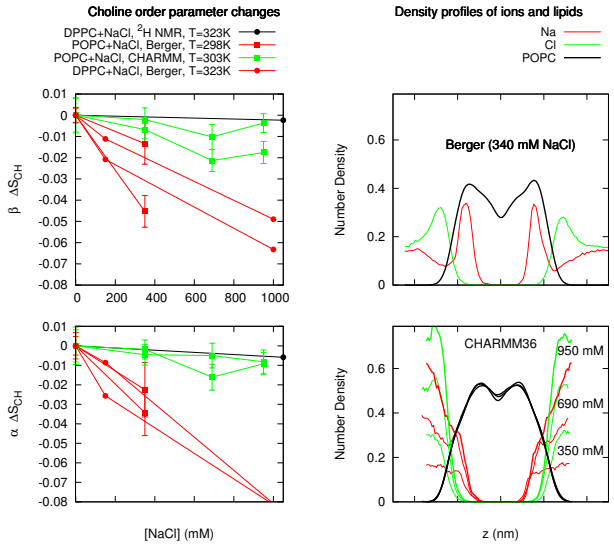

FIG. 7: Changes in choline order parameters (left column) and ion density distributions (right column) as a function of NaCl concentration. Significant order parameter reduction and Na^+ partition is observed with Berger model while only modest order parameter change and ion parition observed with CHARMM36. The results are in line with the electrometer concept connecting the ion partition and choline order parameters changes [42, 66–68]. Consequently, the results show that Na^+ partition is significantly overestimated in the Berger model. For more discussion see [72].

yet fully resolved [23, 24, 26, 29, 132, 133]. Unfortunately the accuracy of atomistic resolution models is not yet sufficient to solve these issues. However, the modeling of interfacial region structure has been getting more attention lately [30, 31, 37, 50, 51], thus higher quality models may be expected.

On the other hand, the increase of choline α and β order parameters with dehydration and decrease with cation penetration were correctly reproduced by several models, despite of inaccurate choline structures [37, 72]. The order parameter increase was related to the choline P–N vector tilting more parallel to the membrane normal [37] and order parameter decrease to the cation binding affinity [72]. The observations are in line with previous studies on charge penetration [42, 66–68]. However, choline structural changes due to cholesterol or ion concentration are significantly overestimated in several models [36, 37, 72, 107], especially Na^+ binding affinity [72] (see also Fig. 7). The artificial specific Na^+ binding induces effectively postively charged membrane which may easily lead to errorneous conclusion due to dominant contribution of electrostatics for various phenomena.

In conclusion, the atomistic resolution MD simulations are invaluable in understanding the structural details and their changes in acyl chain region. However, in applications where lipid interfacial region structure, energetics, electrostatics or ion distributions have significant role, the potential artefacts

arising from simulation models must be cafefully taken into account. A typical example of such application would be a study of interactions between charge containing protein in solution and lipid bilayer, simulated in physiological salt concentration [134, 135].

C-H BOND ROTATIONAL DYNAMICS FROM SPIN RELAXATION RATES AND SIMULATIONS

Definition and properties of rotational auto–correlation function

The second order auto-correlation function for the reorientation of the C–H chemical bond axis is defined as

$$g(\tau) = \langle P_2[\vec{\mu}(t) \cdot \vec{\mu}(t+\tau)]\rangle, \tag{4}$$

where P_2 denotes the second Legendre polynomial, $P_2(\xi) = 1/2(3\xi^2 - 1)$, $\vec{\mu}(t)$ is the unitary vector having the direction of the C–H bond at time t, and the angular brackets denote a time-average. For randomly oriented lamellar structures this autocorrelation is connected to the experimentally measurable spin relaxation rates through its Fourier transformation called spectral density [136].

$$j(\omega) = 2\int_0^\infty \cos(\omega\tau)g(\tau)d\tau. \tag{5}$$

The auto–correlation function for bond orientations always decays to zero with long enough time scales in randomly oriented multilamellar samples due to the diffusion between differently oriented bilayer regions. However, the relaxation processes occur in two distinct timescales and the auto–correlation function can be written as a product of two independent functions [32, 137]

$$g(\tau) = g_{\mathrm{f}}(\tau)g_{\mathrm{s}}(\tau), \tag{6}$$

where $g_{\mathrm{f}}(\tau)$ describes the fast decay (faster than $\sim \mu$s) due to the lipid rotation within bilayer plane and $g_{\mathrm{s}}(\tau)$ describes the slow motions (slower than $\sim \mu$s) from the diffusion between differently oriented bilayer regions. The correlation time of 4.2 ms for the slow decay was estimated from the spin-lattice relaxation rates in rotating frame $R_{1\rho}$, measured with different nutation frequencies for multilamellar POPC sample at 300K [32]. The full auto–correlation decaying to zero, including the contribution from the magic angle spinning (MAS) in kHz region [138], is illustrated in Fig. 8.

The $g_{\mathrm{f}}(\tau)$ decays to the plateau having value of S^2_{CH} within few hundred nanoseconds in liquid crystalline lipid bilayers with planar symmetry [32], as illustrated in Fig 8. The order parameters from ^{2}H NMR and ^{13}C NMR experiments are measured from this plateau [32], thus the rotational correlation function describes the average time needed to sample all conformations for a single molecule within the bilayer plane.

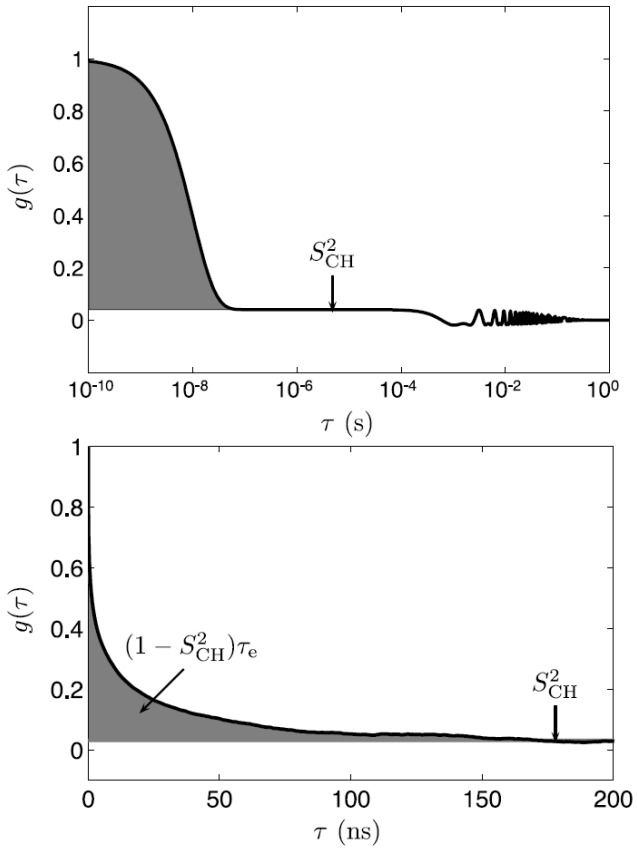

FIG. 8: (Top) Illustration of the auto-correlation function $g(\tau)$ and effective correlation time τ_e for a ^{13}C-H bond in a lipid bilayer in MAS experiment (x–axis with logarithmic scale). Plateau after fast relaxation processes $g(\tau)_f$ is shown between roughly 10^{-7}s and 10^{-4}s. After this timescale the slow relaxation processes $g(\tau)_s$ and oscillation due to MAS [138] are shown. (Bottom) $g(\tau)$ for g_1 segment having the slowest relaxation in POPC bilayer simulated with the Berger based model, illustrating the decay towards S^2_{CH} (x–axis with linear scale). This represents the $g(\tau)_f$ in Eq. 6 and decrease to the plateau in the top figure. The effective correlation time τ_e is equal to the area in gray scaled by $(1 - S^2_{\mathrm{CH}})^{-1}$. Figure adapted from [32].

The effective correlation time [136]

$$\tau_e := \int_0^\infty \frac{g_{\mathrm{f}}(\tau) - S^2_{\mathrm{CH}}}{1 - S^2_{\mathrm{CH}}}\mathrm{d}\tau \tag{7}$$

gives intuitive measure for this time; larger τ_e means longer time required for the conformational sampling. With this definition the area between the correlation function and its pleateau becomes $(1 - S^2_{\mathrm{CH}})\tau_e$, as illustrated in Fig. 8.

Detecting C–H bond dynamics experimentally

The C–H bond dynamics in nanosecond timescales can be detected experimentally by measuring the spin relaxation rates

R_1^C from ^{13}C NMR and R_1^D from ^{2}H NMR. These are connected the molecular dynamics through the spectral density (Eq. 5) and equations [139]

$$R_1^C = \frac{D_{\max}^2 N_{\mathrm{H}}}{20}\Big[j(\omega_{\mathrm{H}}-\omega_{\mathrm{C}})+3j(\omega_{\mathrm{C}})+6j(\omega_{\mathrm{C}}+\omega_{\mathrm{H}})\Big] \quad (8)$$

and

$$R_1^D = \frac{12\pi^2}{40}\left(\frac{e^2qQ}{h}\right)^2\Big[j(\omega_{\mathrm{D}}) + 4j(2\omega_{\mathrm{D}})\Big], \quad (9)$$

where ω_{C}, ω_{H} and ω_{D} are the Larmor frequencies for ^{13}C, ^{1}H and ^{2}H, respectively, N_{H} is the number of bound protons, $\frac{D_{\max}}{2\pi}$ ≈22 kHz as in section 1 and $\frac{e^2qQ}{h}$=170kHz as in section 1.

As seen from Eqs. 8 and 9, the numerical values of R_1^C and R_1^D depend on spectral density values at the Larmor frequencies ω_C, ω_H and ω_D. On the other hand, the spectral density value for a given frequency ω depends on the relative amount of relaxation processes with timescales close to ω^{-1}. The Larmor frequencies depend on the spectrometer magnetic field strength and typical timescales for ω^{-1} are ∼1-20ns in ^{13}C NMR and ^{2}H NMR experiments. Thus, the R_1^C and R_1^D values measured with standard spectrometer with fixed external field stregth gives a measure of relative amount of relaxation processes with the timescales ∼1-20ns. Further, the measured changes gives only the change of the relative amount of dynamical processes with the timescale detected, not the changes in sampling rate. For further discussion and demonstrations see e.g. [32].

For more comprehensive dynamical picture the spin relaxation parameters are measured with different magnetic field strengths by using the field cycling NMR [78, 140–142] and several spectrometers with different magnetic field strengths, as recently reviewed by Leftin and brown [59]. Also the model free approach to measure the effective correlation time (Eq. 7) was recently introduced [32]. The method is based on the combination of experimental order parameter S_{CH}, spin-lattice relaxation rates R_1^C and the transverse magnetization under a spin lock pulse $R_{1\rho}^{\mathrm{plateau}}$ measured with appropriate nutation frequency, given through equation

$$\tau_{\mathrm{e}} \approx \frac{5R_{1\rho}^{\mathrm{plateau}} - 3.82R_1^C}{D_{\max}^2 N_{\mathrm{H}}(1-S_{\mathrm{CH}}^2)}. \quad (10)$$

Analyzing C–H bond dynamics from simulations

Since all the atom coordinates as a function of time are available from molecular dynamics simulations trajectory, the auto–correlation function for each C–H bond can be calculated directly from the definition in Eq. 4. The hydrogen positions can be generated post-simulationally based on heavy atoms positions and the known hydrocarbon geometries for united atom simulations without explicit hydrogens by creating a trajectory with added hydrogens [32, 82, 143, 144]. The ensemble average is taken over all the time intervals and molecules in present in simulation. Since the amount of data decreases for time intervals approaching the simulation total length, only interval lengths less than half of the total simulation time are typically used; for more details see [145].

To calculate the experimentally measurable spin lattice relaxation times from Eqs. 8 and 9, the spectral density must be first calculated from auto-correlation function using Eq. 5. Usually sum of 4 or more exponentials are fitted to the calculated auto–correlation function and then analytical Fourier transform is used to calculate the spectral density [17, 32, 82, 123, 146, 147], however some authors have also used streched exponential exponential functions [143, 144]. The chosen functional form should not affect the spin relaxation rate values as long as the fit is good, however the correct form to describe the real relaxation process can be debated [59, 144, 148–150]. Single exponential function is not enought to describe relaxation observed in simulations while 4 gives a reasonable fit [123] which is not surprising since more than one relaxation timescales are expected to be present in bilayer lipids [17, 59, 146, 147]. The R_1^C and R_1^D values are straighforward to calculate from Eqs. 8 and 9 with different Larmor frequencies or as a function of external field by using the fitted spectral density function.

The effective correlation time τ_e can be calculated directly from the integrated area below the correlation function, see Fig. 8 or by using the exponential sum fitted to the correlation function as in Eq. 30 of Ref. [32]. The $R_{1\rho}$, used to determine effective correlation time experimentally in Eq. 7 cannot be calculated from simulations directly since its value may depend also on the slow relaxation dynamics ($g_s(t)$ in Eq. 6) which is not present in simulations [32]. The same applies to the calculation of NOESY relaxations rates and in this case decay time of 170 ns was assumed for the $g_s(t)$ [151], while 4.2 ms was measured by Ferreira et al. [32].

Comparing C–H bond dynamics between simulations and NMR experiments

Spin relaxation rates R_1^C and R_1^D with one [32, 82, 98, 115, 123] or more [17, 98, 118, 143, 144, 147, 149] external magnetic field strengths have been compared between experiments and simulations mainly for CHARMM (Fig. 9) and Berger based models (Fig. 10). The comparison with several magnetic field strengths shows good a agreement with large larmor frequencies for both CHARMM and Berger based models in Figs. 9 and 10 A), respectively. With increasing larmor frequencies both models show a good agreement deep in the acyl chain region while closer to the interfacial region motional modes corresponding lower Larmor frequencies seems to overpresented in both models. Since lower Larmor frequencies correspond longer correlation times, this may indicate too slow dynamics close to the interfacial region.

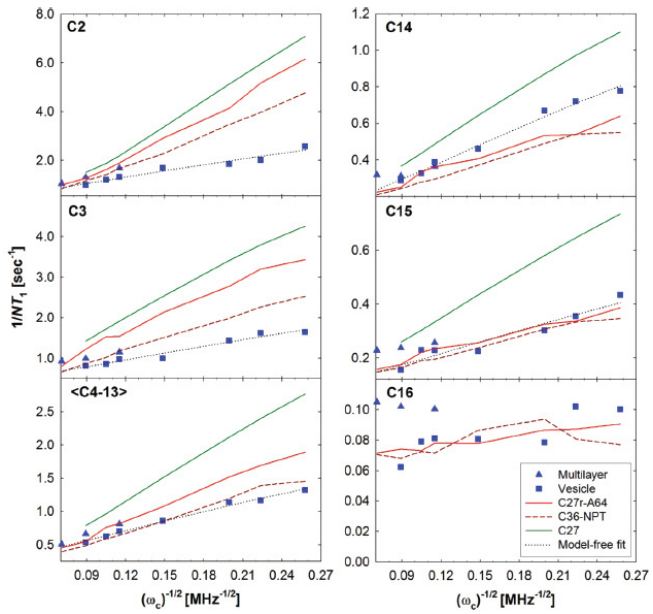

FIG. 9: Comparison of R_1^C dependence on magnetic field between experiments [149, 152] and different CHARMM simulations [50] for acyl chain carbons (DPPC bilayer in 323K) adapted from [50]. Experiments as points; MD simulations as solid and dashed lines; and a model-free fit to the vesicle data as dotted lines.

This is in line with the comparison between experimental and simulated effective correlation times for Berger based POPC model, shown in Fig. 10 C); the effective correlation times for acyl chain region agrees with experiments while closer to the interfacial region the correlation times are too large in simulations. The discrepancies for R_1^C between experiments and simulations for acyl chain region shown in Fig. 10 B) indicate, however, that different dynamical processes are not correctly balanced in simulations despite of good agreement for τ_e. On the other hand, spin relaxation rates for polyunsaturated acyl chains with large Larmor frequenciens give reasonable values for both, CHARMM [118, 123] and Berger based [82] models.

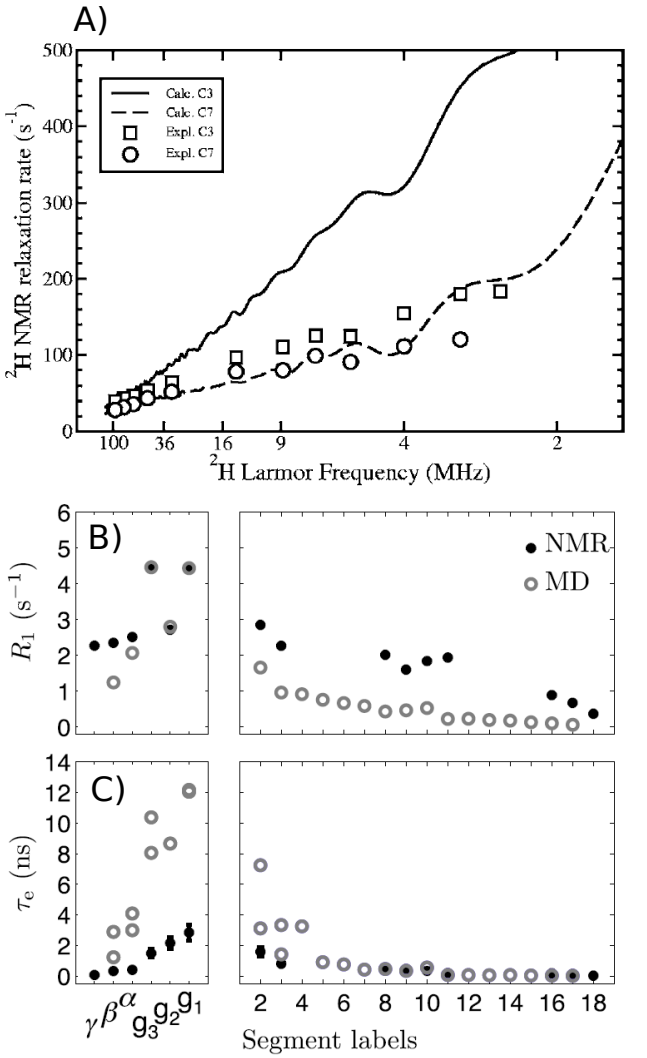

FIG. 10: Comparisons between Berger based models and experimental spin relaxation rates: A) R_1^D dependence on magnetic field for acyl chain carbons (DMPC bilayer at 300K) adapted from [144], B) R_1^C measured with field strength correspondin to the Larmor frequency of 125 MHz for ^{13}C (POPC bilayer at 298K) and C) effective correlation times τ_e (POPC bilayer at 298K) adapted from Ferreira et al. [32].

Interplay between simulations and NMR spin lattice relaxation times: Validation and interpretation of dynamics

Most importantly, the fairly good agreement for spin relaxation rates and effective correlation times between simulations and experiments in acyl chain region indicates that the lipid rotational dynamics has the correct order of magnitude in simulations. Consequently, the rapid acyl chain fluctuations observed in simulations can be considered as realistic which further supports the advantage of simulation videos as intuitive lipid bilayer picture compared to the traditional static pictures. While the molecular sampling rates seems to be underestimated closer to the interface, also the sampled structures are not excatly correct in simulations [37], thus the sampling rates in simulations are mainly interesting only for people improving the models.

As discussed in Section 3 and for example in Ref. [32], single measured spin relaxation rate values or changes are not straightforwardly connected to the molecular dynamics. MD simulations can significantly ease this connection if the experimental spin relaxation rates or their differences can be reproduced [19, 115, 123]. This has been especially useful in the studies of polyunsaturated acyl chain dynamics which concluded – by combining the simulation and NMR relaxation data – that the double bonds speed up the chain dynamics due to flexible dihedrals next to the double bonds [115, 123–125].

The successfull interpretation of relaxation time measure-

ments with MD is significantly less laborious than careful studies with different temperatures and magnetic field strengths, recently reviewed by Leftin and Brown [59]. On the other hand, the interpretation is also eased by the recently introduced effective correlation time experiments [32]. For example, careful compilation of several experimental data sets with different temperatures and magnetic fields was needed to conclude that the lipids has slower dynamics in interfacial region than in the acyl chains region [59], while the same conclusion is obvious from the measured effective correlation times in Fig. 10 [32]. The same is seen also in the MD simulations, however, the simulation model quality is not yet on the level to be used alone for interpretataion for interfacial region.

Lipid bilayer rotational modes have been often interpreted with the wobble in the cone model [17, 78, 147, 149, 150] suggesting that the whole lipid molecule is wobbling as a cone and that all lipid segments share the same time scale for this motion. Further timescales for segmental dynamics then arises from the dynamics inside the cone. The auto–correlation functions predicted by the model are successfully fitted to the simulation and experimental data [17, 78, 147, 149, 150], however, fits with similar or better quality would be probably possible also with other type of models as well. In addition, significant changes of structure and dynamics experienced in the acyl chain region may not hinge on the headgroup [37, 153] indicating weak coupling between these segments, in line with one plausible interpretation for recent field cycling experiments [142], and the role of membrane undulations in the low frequency relaxation data is still under discussion [59, 148–150]. Thus, the wobbling in the cone is not yet fully proven to be the correct description for lipid rotational dynamics. Lipid models with realistic rotational dynamics for all segments with all timescales could elucidate this issue significantly.

FORM FACTORS FROM SCATTERING AND SIMULATIONS

Form factor measured with X-ray or Neutron scattering

Small-angle X-ray or neutron scattering (SAXS/SANS) experiments can be used to probe the overall structure of the lipid bilayer, in particular scattering length density profiles along normal axis. The measured scattering intensity can be written as $I(q) \sim |F(q)|^2 S(q)/C_{\mathrm{LF}}$, where $F(q)$ is the bilayer form factor, $S(q)$ is the structure factor and C_{LF} the Lorentz correction ($C_{\mathrm{LF}} = q^2$ for free-floating lipid vesicles and $C_{\mathrm{LF}} = q$ for aligned bilayers). The structure factor characterizes the crystalline or quasicrystalline structure of bilayer stacks and the form factor describes the scattering length density distribution of the lipid bilayer itself along the bilayer normal.

Here the main interest lies in the form factor since we focus on the lipid bilayer structure. The scattering intensity can be measured from unilamellar vesicles (ULVs) [15], oriented multilamellar bilayes (ORI) [154, 155] and un-oriented multilamellar vesicles (MLVs) [156]. Information about the structure factor is needed to extract the form factor from the scattering intensity, except for positionally uncorrelated ULVs, where $S(q) = 1$ [15]. For multibilayers in the fluid phase the structure factor is given by the Caillé theory [154, 157]. For oriented samples the form factor is determined by scaling a 2D fit of the Caillé structure factor (for in-plane and out-of-plane scattering constributions) to the measured scattering intensity [154, 155]. For MLVs the form factor needs to be modeled in combination with the structure factor to fit the scattering intensity [156]. This is achieved by using a specific real-space description of the bilayer structure (scattering length density profile). Note that different real-space model yield equivalent form factors. Thus, the form factors are not highly sensitive to the applied model. Different technical issues must be carefully considered in all scattering experiments, in particular subtracting background scattering and, in the case of ORI and MLVs, fitting accuracy. The form factors measured from different geometries [155, 158, 159] and research groups are in good agreement as demonstrated in Fig. 11, indicating that the bilayer structure is similar in different preparations of the same lipid and that the technique is highly robust.

By following the notation from Ref. [33], the form factor is connected to the bilayer atom number density through the equation

$$|F(q)| = |\int_{-D/2}^{D/2} (\sum_{\alpha} f_\alpha(q_z) n_\alpha(z) - \rho_s) \exp(izq_z) \mathrm{d}z|, \tag{11}$$

where $n_\alpha(z)$ in the atom α number density as a function of membrane normal coordinate z, $f_\alpha(q_z)$ is the atom scattering length density, ρ_s is the solvent scattering length density and integral spans over the bilayer of thickness D. The atom scattering length density $f_\alpha(q_z)$ depends on the type of scattering used since X-ray photons interact with the sample's electron cloud, while neutron scatter off nuclei in a particular manner. This leads also to distinct contrast for different parts of the membrane. X-rays, for example are most sensitive to the electron-rich phospholipid headgroups. Neutron experiments typically explore the contrast between hydrogen and deuterium [15], e.g. SANS on protiated lipid bilayers suspended in 100% D_2O probes mainly the membrane's hydrophobic thickness and specifically deutreated lipids are used to study lipid structural details [160, 161]. Also, e.g. ^{44}Ca has been used to detect Calcium location in lipid bilayer [162]. Consequently, highest-structural resolution can be achieved upon combining SAXS and SANS experiments [155, 163].

For symmetric lipid bilayers Eq. 11 simplifies to the widely used form

$$|F(q)| = |\int_{-D/2}^{D/2} \Delta\rho_e(z) \cos(zq_z) \mathrm{d}z|, \tag{12}$$

where $\Delta\rho_e(z)$ is the scattering length density difference between solvent and bilayer.

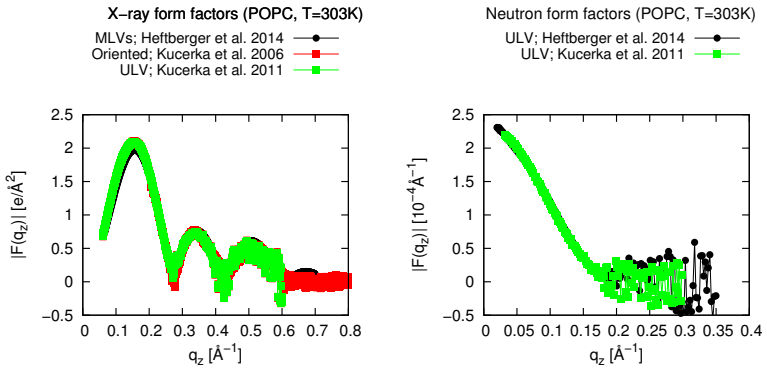

FIG. 11: Comparison of reported X-ray (Panel A) and neutron (Panel B) form factors for POPC bilayers at 303K in different geometries measured in different groups.

Form factor calculation from simulations

The atomic number densities $n_\alpha(z)$ are straighforward to calculate from simulations and then substitute into Eq. 11 to calculate the form factor. The atomic scattering length densities $f_\alpha(q_z)$ for neutrons are available in the literature [164]. For x-ray scattering pointwise valence electron location at the atom positions is usually assumed and in this case the $f_\alpha(q_z)$ becomes the number of electron per atom, while also gaussian electron distribution around atom positions [165] or an analytical expression $f_\alpha(q_z) = \sum_{j=1}^{4} a_j e^{-b_j(q/4\pi)^2} + c$ with parameters a_j, b_j and c taken from [166] are assumed in some studies [165], including the widely used SIMtoEXP software [33]. The effect of these choices to the electron density profiles was discussed by Benz et al. [165], however, it is not clear how strongly this would affect form factors calculated from simulations. In most simulations the bilayer is symmetric, thus the simpler Eq. 12 is used.

The small bilayer patches used in simulations might depress bilayer undulation modes which are present in large scale experiments [167]. Braun et al. showed that undulations seen in large simulations do not change the location of form factor minimas but depress the peak hights in the lobes [167]. Since the undulations are expected to be present in the experiments, the potential discrepancies between simulations and experiments in the lobe heights may be explained by the lack of undulation motions in simulations. The undulation effects are also sometimes reduced from the experimentally reported form factors by scaling q in x–axis, however, the scaling factor is very close to 1 [155].

Simulations give the form factors on absolute scale while experiments obtain them only on a relative scale, thus the experimental form factors from different sources has to be scaled for comparison [33, 163]. For example, the SIMtoEXP program uses the scaling factor k defined as

$$k = \frac{\sum_{i=1}^{N} \frac{|F_s(q_i)||F_e(q_i)|}{(\Delta F_e(q_i))^2}}{\sum_{i=1}^{N} \frac{|F_e(q_i)|^2}{(\Delta F_e(q_i))^2}}, \qquad (13)$$

where $F_e(q)$ and $F_s(q)$ are experimental and simulated form factors, respectively, $\Delta F_e(q)$ is the uncertainty of the experimental form factor and the summation goes over all N data points [33, 163].

Comparing form factors between simulations and experiments

The comparison to experimental area per molecule values to validate the lipid density in simulations [83] has been nowdays often replaced with more direct comparison [5] using x-ray form factors [30, 45, 49–56, 105–107, 118, 119]. In some studies the comparison is complemented with the comparison to the neutron scattering data with D_2O [51, 52, 54–56, 107]. In general the models produce form factors in good agreement with experiments, especially at small q values indicating that the overall bilayer dimensions, like thickness, are reproduced reasonably well. However, the agreement gets often worse toward higher q values [30, 49–53, 55, 56, 105–107, 118, 119] (see Fig. 12), indicating discrepancies in fine structural details such as, e.g. hydrocarbon chain packing or headgroup structure. Typically, the comparison of experimental and simulated form factors is based on visual inspection while also quantitative measure for simulated form factor quality has been suggested [33]. In some studies also Fourier transform coeffiecients are compared [165]

Also changes in form factor due to temperature [52, 108], cholesterol concentration [106, 107] and acyl chain polyunsaturation [118, 123] have been compared between simulations and experiments [14, 123, 155, 168–172]. Simulation generally reproduce the decreased thickness and increased area with increasing temperature [52, 108] and polyunsaturation level [118, 123], as well as increased thickness and decreased

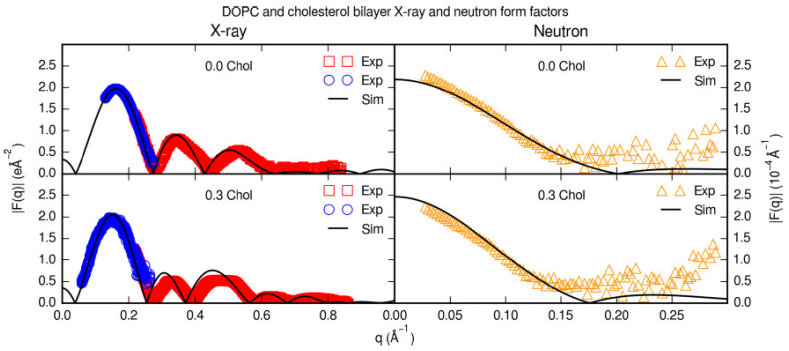

FIG. 12: Example of comparison between simulation model and experiment. The agreement is better with low q values and cholesterol induced thickening is overestimated. Figure adapted from Madej et al. [107].

area with increasing cholesterol concentration [106, 107]. However, the temperature dependence is underestimated for some systems [52, 108] while cholesterol effect is overestimated [106, 107]. Example of such comparison is shown in Fig. 12.

In conclusion, all the state of the art simulation models gives form factors close to experimental data in various conditions indicating reasonable agreement for average bilayer dimensions. Also the qualitative changes are reproduced, however, discrepancies prevail for quantitative details of bilayer structure and changes with temperature and admixture of other lipids such as cholesterol.

Interplay between simulations and scattering experiments: Validation and interpretation

The scattering form factor gives accurate information about lipid bilayer structure but a model for atom number densities, $n_\alpha(z)$ in Eq. 11, is needed to resolve the structure, analogously to the NMR order parameters. Further, several atom density profiles can reproduce essentially the same form factor [163], thus also independent information is needed to confirm the structures suggested by the models, also analogously to the NMR order parameters. As already discussed in Section 1, significant advantage of MD model is that the same model can be straightforwardly compared to both, NMR and scattering data.

Several models, reviewed by Heberle et al. [173], are developed to give structural interpretation for the form factor data [174], while also MD simulations are used [163, 175–178]. In these studies the area per molecule is often fixed to a value minimizing the differences between experimental and simulated form factors [163, 175–178]. Depending on the model used, this area per molecule may be close to [178] or deviate significantly [163, 175–177] from the value predicted by the model in constant pressure simulations. However, with optimized area per molecule all models give form factors close to the experiments, despite of the bilayer tension generated in some models. On the other hand, comparisons between MD simulations and SDP model suggest small but measurable structural differences [163, 178]. The form factor from SDP model agrees better with experiments and stuctural parameters indicate differences especially in the glycerol backbone and the headgroup regions [163, 178], in agreement with comparison between simulations and NMR order parameters [37], as discussed in section 3.

CONCLUSIONS

The comparisons of lipid bilayer C–H bond order parameters, spin relaxation rates and scattering form factors between MD simulations and experiments for the validation and interpretation of the sampled atomistic resolution structures are reviewed. The segmental order parameters and spin relaxation rates, measured with NMR, are related to the sampled structure and dynamics of individual molecules, while the scattering form factor is related to the average structure of the whole bilayer. NMR and scattering experiments are both highly robust and directly comparable to simulations, thus the sampled lipid and bilayer structures in MD model can be realistic only if these experimental quantities are reproduced with sufficient accuracy. Such an MD simulation model would be an ultimate tool to jointly interpretate the NMR and scattering data. Further, such a model reproducing numerous independent experimental observables could be considered as the realistic atomistic resolution representation with high probability.

The current MD simulation models are not quite yet cabable for this, however, with current computational resources and available experimental data the community has a fair change to create truly realistic atomistic resolution representations of lipid bilayers. More specifically:
- Atomistic resolution MD simulations give realistic structures and rotational dynamics with correct order of magnitude for saturated and unsaturated acyl chains for PC lipid bilayers in full hydration close to 300K (or 323K for DPPC). Thus, the videos given by simulations can be considered as a realistic

intuitive picture about the acyl chain region.
- Qualitative changes in the acyl chain region with temperature, dehydration and cholesterol are correctly described, however, in many cases the quality of atomistic resolution details of the changes are not clear.
- Current MD simulations are not yet accurate enough to resolve the atomistic resolution properties of glycerol backbone and choline regions, however, some structural changes can be correctly reproduced. Extreme care must be taken when simulation results are used to study, e.g. lipid–ion or lipid–cholesterol interactions on this region.

Similar conclusions are often made from the comparisons between simulations and two complementary experimental techniques, NMR and scattering, the first one related to the average properties of individual molecules and the latter to the average bilayer properties. In wider perspective it seems that atomistic MD simulations, NMR spectroscopy and scattering all gives complementary and coherent information on atomistic resolution biomolecular structure and dynamics. This indicates that the combination of these techniques has a realistic potential to generate atomistic resolution dynamical models of biomolecules in biologically relevant fluid state, however, the main current barrier seems to be quality of the interactions described in the MD model.

The demand for atomistically accurate MD models will most likely increase in near future with increasing amount of accurate experimental data due the development in NMR methodology for lipids [32, 36, 61, 62] and proteins [179], as well as due to, e.g. wide-angle x-ray scattering of lipid bilayers, probing short-range positional correlations between hydrocarbons [180].

The inaccuracies of simulation models in the interfacial region may also hamper the simulation studies of different biochemical systems. For example, protein approaching PC lipid bilayer in physiological NaCl concentration may approach an effectively positively charged lipid bilayer due to artificial Na^+ binding with incorrect choline structure. In addition, the protein might sample incorrect states already in the bulk water [181–183]. From such a simulation it is difficult to filter results arising purely from simulation artefacts.

* samuli.ollila@aalto.fi
† BioTechMed-Graz, Graz, Austria

[1] J. N. Israelachvili, S. Marcelja, and R. G. Horn, Q. Rev. Biophys. **13**, 121 (1980).
[2] R. E. Jacobs and E. Oldfield, Prog. Nucl. Mag. Res. Sp. **14**, 113 (1981).
[3] J. H. Davis, Biochim. Biophys. Acta **737**, 117 (1983).
[4] M. Bloom, E. Evans, and O. G. Mouritsen, Quarterly Reviews of Biophysics **24**, 293 (1991), ISSN 1469-8994, URL http://journals.cambridge.org/article_S0033583500003735.
[5] J. F. Nagle and S. Tristram-Nagle, Biochem. Biophys. Acta **1469**, 159 (2000).
[6] J. F. Nagle, Faraday Discuss. **161**, 11 (2013).
[7] A. G. Lee, Biochim. Biophys. Acta **1666**, 62 (2004).
[8] P. K. J. Kinnunen, The Open Biology Journal **2**, 163 (2009).
[9] M. Bohdanowicz and S. Grinstein, Physiological Reviews **93**, 69 (2013), ISSN 0031-9333.
[10] J. Seelig, Q. Rev. Biophys. **10**, 353 (1977).
[11] H. U. Gally, G. Pluschke, P. Overath, and J. Seelig, Biochemistry **20**, 1826 (1981).
[12] P. Scherer and J. Seelig, The EMBO journal **6** (1987).
[13] G. Pabst, N. Kucerka, M.-P. Nieh, M. Rheinstdter, and J. Katsaras, Chem Phys Lipids **163**, 460 (2010), ISSN 0009-3084, URL http://www.sciencedirect.com/science/article/B6T2N-4YRHCWP-1/2/539e61bf10683661bd62b21d109fcb9a.
[14] N. Kučerka, M. P. Nieh, and J. Katsaras, Biochim Biophys Acta **1808**, 2761 (2011), ISSN 0006-3002.
[15] D. Marquardt, F. A. Heberle, J. D. Nickels, G. Pabst, and J. Katsaras, Soft Matter (2015).
[16] P. van der Ploeg and H. J. C. Berendsen, The Journal of Chemical Physics **76**, 3271 (1982), URL http://scitation.aip.org/content/aip/journal/jcp/76/6/10.1063/1.443321.
[17] R. W. Pastor, R. M. Venable, M. Karplus, and A. Szabo, The Journal of Chemical Physics **89**, 1128 (1988), URL http://scitation.aip.org/content/aip/journal/jcp/89/2/10.1063/1.455219.
[18] J. Kapla, B. Stevensson, M. Dahlberg, and A. Maliniak, J. Phys. Chem. B **116**, 244 (2012).
[19] A. Nowacka, N. Bongartz, O. Ollila, T. Nylander, and D. Topgaard, Journal of Magnetic Resonance **230**, 165 (2013).
[20] T. M. Ferreira, D. Topgaard, and O. H. S. Ollila, Langmuir **30**, 461 (2014).
[21] A. Abragam, *The Principles of Nuclear Magnetism* (Oxford University Press, 1961).
[22] A. Seelig and J. Seelig, Biochemistry **13**, 4839 (1974).
[23] H. U. Gally, W. Niederberger, and J. Seelig, Biochemistry **14**, 3647 (1975).
[24] A. Seelig and J. Seelig, Biochemistry **16**, 45 (1977).
[25] J. Seelig and N. Waespe-Sarcevic, Biochemistry **17**, 3310 (1978).
[26] L. Strenk, P. Westerman, and J. Doane, Biophys. J. **48**, 765 (1985).
[27] J. E. Baenziger, H. C. Jarrel, R. J. Hill, and I. C. P. Smith, Biochemistry **30**, 894 (1991).
[28] M. Hong, K. Schmidt-Rohr, and D. Nanz, Biophys. J. **69**, 1939 (1995).
[29] K. S. Bruzik and J. S. Harwood, Journal of the American Chemical Society **119**, 6629 (1997).
[30] J. Chowdhary, E. Harder, P. E. M. Lopes, L. Huang, A. D. MacKerell, and B. Roux, J. Phys. Chem. B **117**, 9142 (2013).
[31] P. Prakash and R. Sankararamakrishnan, J. Comp. Chem. **31**, 266 (2010).
[32] T. M. Ferreira, O. H. S. Ollila, R. Pigliapochi, A. P. Dabkowska, and D. Topgaard, J. Chem. Phys. **142**, 044905 (2015), URL http://scitation.aip.org/content/aip/journal/jcp/142/4/10.1063/1.4906274.
[33] N. Kuerka, J. Katsaras, and J. Nagle, Journal of Membrane Biology **235**, 43 (2010), ISSN 0022-2631.
[34] J. D. Gross, D. E. Warschawski, and R. G. Griffin, J. Am. Chem. Soc. **119**, 796 (1997).
[35] S. V. Dvinskikh, V. Castro, and D. Sandstrom, Phys. Chem. Chem. Phys. **7**, 607 (2005).
[36] T. M. Ferreira, F. Coreta-Gomes, O. H. S. Ollila, M. J.

Moreno, W. L. C. Vaz, and D. Topgaard, Phys. Chem. Chem. Phys. **15**, 1976 (2013).
[37] A. Botan, F. Fernando, J. F. Patrick Franois, M. Javanainen, M. Kanduc, W. Kulig, A. Lamberg, C. Loison, A. P. Lyubartsev, M. S. Miettinen, et al., The Journal of Physical Chemistry B **0**, null (0), pMID: 26509669, http://dx.doi.org/10.1021/acs.jpcb.5b04878, URL http://dx.doi.org/10.1021/acs.jpcb.5b04878.
[38] M. Hong, K. Schmidt-Rohr, and A. Pines, J. Am. Chem. Soc. **117**, 3310 (1995).
[39] A. Seelig and J. Seelig, Biochimica et Biophysica Acta (BBA) - Biomembranes **406**, 1 (1975).
[40] A. K. Engel and D. Cowburn, FEBS Letters **126**, 169 (1981).
[41] B. Perly, I. C. P. Smith, and H. C. Jarrell, Biochemistry **24**, 1055 (1985).
[42] H. Akutsu and J. Seelig, Biochemistry **20**, 7366 (1981).
[43] B. Bechinger and J. Seelig, Chem. Phys. Lipids **58**, 1 (1991).
[44] O. Berger, O. Edholm, and F. Jähnig, Biophys. J. **72**, 2002 (1997).
[45] C.-J. Högberg, A. M. Nikitin, and A. P. Lyubartsev, J. Comput. Chem. **29**, 2359 (2008).
[46] D. Poger, W. F. Van Gunsteren, and A. E. Mark, J. Comput. Chem. **31**, 1117 (2010).
[47] J. P. Ulmschneider and M. B. Ulmschneider, J. Chem. Theory Comput. **5**, 1803 (2009).
[48] A. Kukol, J. Chem. Theory Comput. **5**, 615 (2009).
[49] S.-W. Chiu, S. A. Pandit, H. L. Scott, and E. Jakobsson, J. Phys. Chem. B **113**, 2748 (2009).
[50] J. B. Klauda, R. M. Venable, J. A. Freites, J. W. O'Connor, D. J. Tobias, C. Mondragon-Ramirez, I. Vorobyov, A. D. M. Jr, and R. W. Pastor, J. Phys. Chem. B **114**, 7830 (2010).
[51] C. J. Dickson, L. Rosso, R. M. Betz, R. C. Walker, and I. R. Gould, Soft Matter **8**, 9617 (2012).
[52] J. P. M. Jämbeck and A. P. Lyubartsev, J. Phys. Chem. B **116**, 3164 (2012).
[53] A. Maciejewski, M. Pasenkiewicz-Gierula, O. Cramariuc, I. Vattulainen, and T. Rog, J. Phys. Chem. B **118**, 4571 (2014).
[54] R. Tjörnhammar and O. Edholm, J. Chem. Theory Comput. **10**, 5706 (2014).
[55] C. J. Dickson, B. D. Madej, . A. Skjevik, R. M. Betz, K. Teigen, I. R. Gould, and R. C. Walker, J. Chem. Theory Comput. **10**, 865 (2014).
[56] S. Lee, A. Tran, M. Allsopp, J. B. Lim, J. Henin, and J. B. Klauda, J. Phys. Chem. B **118**, 547 (2014).
[57] V. Castro, S. V. Dvinskikh, G. Widmalm, D. Sandstrm, and A. Maliniak, Biochimica et Biophysica Acta (BBA) - Biomembranes **1768**, 2432 (2007).
[58] V. Castro, B. Stevensson, S. V. Dvinskikh, C.-J. Högberg, A. P. Lyubartsev, H. Zimmermann, D. Sandström, and A. Maliniak, Biochim. Biophys. Acta - Biomembranes **1778**, 2604 (2008).
[59] A. Leftin and M. F. Brown, Biochim. Biophys. Acta - Biomembranes **1808**, 818 (2011).
[60] D. Marsh, *Handbook of Lipid Bilayers, Second Edition* (RSC press, 2013).
[61] A. Leftin, C. Job, K. Beyer, and M. F. Brown, Journal of Molecular Biology **425**, 2973 (2013).
[62] A. Leftin, T. Molugu, C. Job, K. Beyer, and M. Brown, Biophysical Journal **107**, 2274 (2014).
[63] J. Douliez, A. Lonard, and E. Dufourc, Biophysical Journal **68**, 1727 (1995), ISSN 0006-3495, URL http://www.sciencedirect.com/science/article/pii/S0006349595803504.
[64] A. Ulrich and A. Watts, Biophys. J. **66**, 1441 (1994).
[65] K. Mallikarjunaiah, A. Leftin, J. J. Kinnun, M. J. Justice, A. L. Rogozea, H. I. Petrache, and M. F. Brown, Biophysical Journal **100**, 98 (2011), ISSN 0006-3495, URL http://www.sciencedirect.com/science/article/pii/S0006349510013792.
[66] C. Altenbach and J. Seelig, Biochemistry **23**, 3913 (1984).
[67] J. Seelig, P. M. MacDonald, and P. G. Scherer, Biochemistry **26**, 7535 (1987).
[68] P. G. Scherer and J. Seelig, Biochemistry **28**, 7720 (1989).
[69] M. F. Brown and J. Seelig, Biochemistry **17**, 381 (1978).
[70] E. Kuchinka and J. Seelig, Biochemistry **28**, 4216 (1989).
[71] M. Roux and M. Bloom, Biochemistry **29**, 7077 (1990).
[72] A. Catte, M. Girych, M. Javanainen, M. S. Miettinen, L. Monticelli, J. Määttä, V. S. Oganesyan, and O. H. S. Ollila, *The electrometer concept and binding of cations to phospholipid bilayers* (2015), dOI: 10.5281/zenodo.32175.
[73] F. Aussenac, M. Laguerre, J.-M. Schmitter, and E. J. Dufourc, Langmuir **19**, 10468 (2003).
[74] G. Raffard, S. Steinbruckner, A. Arnold, J. H. Davis, and E. J. Dufourc, Langmuir **16**, 7655 (2000).
[75] C. R. Sanders and J. P. Schwonek, Biochemistry **31**, 8898 (1992).
[76] L. E. Marbella, B. Yin, and M. M. Spence, The Journal of Physical Chemistry B **119**, 4194 (2015).
[77] J. Becker, A. Comotti, R. Simonutti, P. Sozzani, and K. Saalwchter, The Journal of Physical Chemistry B **109**, 23285 (2005).
[78] V. N. Sivanandam, J. Cai, A. G. Redfield, and M. F. Roberts, Journal of the American Chemical Society **131**, 3420 (2009).
[79] S. V. Dvinskikh, V. Castro, and D. Sandstrom, Phys. Chem. Chem. Phys. **7**, 3255 (2005).
[80] C.-J. Hgberg, , and A. P. Lyubartsev*, The Journal of Physical Chemistry B **110**, 14326 (2006).
[81] *The nmrlipids project, on the signs of the order parameters* (2014), URL http://web.archive.org/web/20150414085027/http://nmrlipids.blogspot.fi/2014/04/on-signs-of-order-parameters.html.
[82] S. Ollila, M. T. Hyvönen, and I. Vattulainen, J. Phys. Chem. B **111**, 3139 (2007).
[83] D. P. Tieleman, S. J. Marrink, and H. J. C. Berendsen, Biochim. Biophys. Acta **1331**, 235 (1997).
[84] L. Vermeer, B. de Groot, V. Rat, A. Milon, and J. Czaplicki, Eur. Biophys. J. **36**, 919 (2007), ISSN 0175-7571, URL http://dx.doi.org/10.1007/s00249-007-0192-9.
[85] D. Poger and A. E. Mark, J. Chem. Theory Comput. **8**, 4807 (2012).
[86] M. Bachar, P. Brunelle, D. P. Tieleman, and A. Rauk, J. Phys. Chem. B **108**, 7170 (2004).
[87] J. Wong-ekkabut, Z. Xu, W. Triampo, I.-M. Tang, D. P. Tieleman, and L. Monticelli, Biophysical Journal **93**, 4225 (2007), ISSN 0006-3495, URL http://www.sciencedirect.com/science/article/pii/S0006349507716752.
[88] A. Vogel and S. Feller, The Journal of Membrane Biology **245**, 23 (2012), ISSN 0022-2631.
[89] E. Egberts and H. J. C. Berendsen, J. Chem. Phys. **89**, 3718 (1988).
[90] T. R. Stouch, Molecular Simulation **10**, 335 (1993).
[91] E. Egberts, S.-J. Marrink, and H. Berendsen, European Biophysics Journal **22**, 423 (1994), ISSN 0175-7571, URL http://dx.doi.org/10.1007/BF00180163.
[92] J. W. Essex, M. M. Hann, and W. G. Richards, Philos. T. Roy. Soc. B **344**, 239 (1994).

[93] A. Robinson, W. Richards, P. Thomas, and M. Hann, Biophys. J. **67**, 2345 (1994).

[94] M. T. Hyvönen, M. Ala-Korpela, J. Vaara, T. T. Rantala, and J. Jokisaari, Chem. Phys. Lett. **246**, 300 (1995).

[95] V. Kothekar, Ind. J. Biochem. Biophys. **33**, 431 (1996).

[96] D. P. Tieleman and H. J. C. Berendsen, J. Chem. Phys. **105**, 4871 (1996).

[97] W. Shinoda, N. Namiki, and S. Okazaki, J. Chem. Phys. **106**, 5731 (1997).

[98] J. B. Klauda, R. M. Venable, A. D. M. Jr., and R. W. Pastor, in *Computational Modeling of Membrane Bilayers*, edited by S. E. Feller (Academic Press, 2008), vol. 60 of *Current Topics in Membranes*, pp. 1 – 48.

[99] S. W. I. Siu, R. Vcha, P. Jungwirth, and R. A. Bckmann, The Journal of Chemical Physics **128** (2008).

[100] E. J. Dufourc, E. J. Parish, S. Chitrakorn, and I. C. P. Smith, Biochemistry **23**, 6062 (1984).

[101] M. Lafleur, P. Cullis, and M. Bloom, European Biophysics Journal **19**, 55 (1990), ISSN 0175-7571, URL http://dx.doi.org/10.1007/BF00185086.

[102] J. A. Urbina, S. Pekerar, H. biao Le, J. Patterson, B. Montez, and E. Oldfield, Biochimica et Biophysica Acta (BBA) - Biomembranes **1238**, 163 (1995), ISSN 0005-2736, URL http://www.sciencedirect.com/science/article/pii/000527369500117L.

[103] R. J. Mashl, H. L. Scott, S. Subramaniam, and E. Jakobsson, Biophys. J. **81**, 3005 (2001).

[104] Q. Zhu, K. H. Cheng, and M. W. Vaughn, J. Phys. Chem. B **111**, 11021 (2007).

[105] J. B. Lim, B. Rogaski, and J. B. Klauda, J. Phys. Chem. B **116**, 203 (2012).

[106] J. P. M. Jambeck and A. P. Lyubartsev, Phys. Chem. Chem. Phys. **15**, 4677 (2013).

[107] B. D. Madej, I. R. Gould, and R. C. Walker, The Journal of Physical Chemistry B **119**, 12424 (2015).

[108] X. Zhuang, J. R. Makover, W. Im, and J. B. Klauda, Biochimica et Biophysica Acta (BBA) - Biomembranes **1838**, 2520 (2014).

[109] M. Höltje, T. Förster, B. Brandt, T. Engels, W. von Rybinski, and H.-D. Höltje, Biochim. Biophys. Acta **1511**, 156 (2001).

[110] M. T. Hyvönen, T. T. Rantala, and M. Ala-Korpela, Biophys. J. **73**, 2907 (1997).

[111] M. Hyvnen, M. Ala-Korpela, J. Vaara, T. T. Rantala, and J. Jokisaari, Chemical Physics Letters **268**, 55 (1997), ISSN 0009-2614, URL http://www.sciencedirect.com/science/article/pii/S0009261497001711.

[112] S. Feller, D. Yin, R. Pastor, and A. M. Jr, Biophysical Journal **73**, 2269 (1997).

[113] L. Saiz and M. L. Klein, Biophys. J. **204**, 204 (2001).

[114] T. Huber, K. Rajamoorthi, V. F. Kurze, K. Beyer, and M. F. Brown, J. Am. Chem. Soc. **124**, 298 (2002).

[115] S. E. Feller, K. Gawrisch, and A. D. MacKerell Jr., J. Am. Chem. Soc. **124**, 318 (2002).

[116] T. Rg, K. Murzyn, R. Gurbiel, Y. Takaoka, A. Kusumi, and M. Pasenkiewicz-Gierula, Journal of Lipid Research **45**, 326 (2004).

[117] M. T. Hyvönen and P. T. Kovanen, Eur. Biophys. J. **34**, 294 (2005).

[118] J. B. Klauda, V. Monje, T. Kim, and W. Im, The Journal of Physical Chemistry B **116**, 9424 (2012).

[119] W. Kulig, M. Pasenkiewicz-Gierula, and T. Róg, Chem. Phys. Lipids pp. *In Press, Accepted Manuscript, http://dx.doi.org/10.1016/j.chemphyslip.2015.07.002* (2015), URL http://www.sciencedirect.com/science/article/pii/S0009308415300074.

[120] H. I. Petrache, S. W. Dodd, and M. F. Brown, Biophys. J. **79**, 3172 (2000).

[121] K. Rajamoorthi and M. F. Brown, Biochemistry **30**, 4204 (1991).

[122] H. Schindler and J. Seelig, Biochemistry **14**, 2283 (1975).

[123] N. V. Eldho, S. E. Feller, S. Tristram-Nagle, I. V. Polozov, and K. Gawrisch, J. Am. Chem. Soc. **125**, 6409 (2003).

[124] W. Stillwell and S. R. Wassall, Chem. Phys. Lipids **126**, 1 (2003).

[125] K. Gawrisch, N. V. Eldho, and L. L. Holte, Lipids **38**, 445 (2003).

[126] J. H. Ipsen, G. Karlstrm, O. Mourtisen, H. Wennerstrm, and M. Zuckermann, Biochimica et Biophysica Acta (BBA) - Biomembranes **905**, 162 (1987).

[127] T. Rog, M. Pasenkiewicz-Gierula, I. Vattulainen, and M. Karttunen, Biochim. Biophys. Acta **1788**, 97 (2009).

[128] P. Somerharju, J. A. Virtanen, K. H. Cheng, and M. Hermansson, Biochim. Biophys. Acta - Biomembranes **1788**, 12 (2009).

[129] T. Rg and I. Vattulainen, Chemistry and Physics of Lipids **184**, 82 (2014).

[130] A. J. Sodt, M. L. Sandar, K. Gawrisch, R. W. Pastor, and E. Lyman, Journal of the American Chemical Society **136**, 725 (2014).

[131] K. Gawrisch, D. Ruston, J. Zimmerberg, V. Parsegian, R. Rand, and N. Fuller, Biophysical Journal **61**, 1213 (1992).

[132] H. Akutsu and T. Nagamori, Biochemistry **30**, 4510 (1991).

[133] D. J. Semchyschyn and P. M. Macdonald, Magn. Res. Chem. **42**, 89 (2004).

[134] A. Arkhipov, Y. Shan, R. Das, N. Endres, M. Eastwood, D. Wemmer, J. Kuriyan, and D. Shaw, Cell **152**, 557 (2013).

[135] K. Kaszuba, M. Grzybek, A. Orowski, R. Danne, T. Rg, K. Simons, . Coskun, and I. Vattulainen, Proceedings of the National Academy of Sciences **112**, 4334 (2015).

[136] G. Lipari and A. Szabo, J. Am. Chem. Soc. **104**, 4546 (1982).

[137] B. Halle and H. Wennerstrm, The Journal of Chemical Physics **75**, 1928 (1981).

[138] A. Nowacka, P. C. Mohr, J. Norrman, R. W. Martin, and D. Topgaard, Langmuir **26**, 16848 (2010).

[139] R. Harris, *Nuclear magnetic resonance spectroscopy* (John Wiley and Sons Inc.,New York, NY, 1986).

[140] M. F. Roberts, , and . Alfred G. Redfield*, Journal of the American Chemical Society **126**, 13765 (2004).

[141] M. F. Roberts and A. G. Redfield, Proceedings of the National Academy of Sciences of the United States of America **101**, 17066 (2004).

[142] M. F. Roberts, A. G. Redfield, and U. Mohanty, Biophys. J. **97**, 132 (2009).

[143] E. Lindahl and O. Edholm, J. Chem. Phys. **115**, 4938 (2001).

[144] J. Wohlert, W. K. den Otter, O. Edholm, and W. J. Briels, J. Chem. Phys. **124**, 154905 (2006).

[145] M. Abraham, D. van der Spoel, E. Lindahl, B. Hess, and the GROMACS development team, *GROMACS user manual version 5.0.7* (2015), URL www.gromacs.org.

[146] R. Venable, Y. Zhang, B. Hardy, and R. Pastor, Science **262**, 223 (1993).

[147] R. W. Pastor*, , R. M. Venable, and S. E. Feller, Accounts of Chemical Research **35**, 438 (2002).

[148] O. Edholm, in *Computational Modeling of Membrane Bilayers*, edited by S. E. Feller (Academic Press, 2008), vol. 60 of *Current Topics in Membranes*, pp. 91 – 110.

[149] J. B. Klauda, N. V. Eldho, , K. Gawrisch, B. R. Brooks, , and R. W. Pastor*, The Journal of Physical Chemistry B **112**, 5924

(2008).
[150] J. B. Klauda, M. F. Roberts, A. G. Redfield, B. R. Brooks, and R. W. Pastor, Biophysical Journal **94**, 3074 (2008), ISSN 0006-3495, URL http://www.sciencedirect.com/science/article/pii/S0006349508704648.
[151] S. E. Feller, D. Huster, , and K. Gawrisch, Journal of the American Chemical Society **121**, 8963 (1999).
[152] M. F. Brown, A. A. Ribeiro, and G. D. Williams, Proceedings of the National Academy of Sciences **80**, 4325 (1983).
[153] T. M. Ferreira, Ph.D. thesis, Lund University, http://lup.lub.lu.se/record/3878850/file/3879121.pdf (2013).
[154] Y. Lyatskaya, Y. Liu, S. Tristram-Nagle, J. Katsaras, and J. F. Nagle, Phys Rev E **63**, 11907 (2001).
[155] N. Kuerka, Y. Liu, N. Chu, H. I. Petrache, S. Tristram-Nagle, and J. F. Nagle, Biophysical Journal **88**, 2626 (2005).
[156] P. Heftberger, B. Kollmitzer, F. A. Heberle, J. Pan, M. Rappolt, H. Amenitsch, N. Kučerka, J. Katsaras, and G. Pabst, Journal of Applied Crystallography **47**, 173 (2014), URL 24587787.
[157] R. Zhang, R. M. Suter, and J. F. Nagle, Phys Rev E **50**, 5047 (1994).
[158] N. Kučerka, S. Tristam-Nagle, and J. F. Nagle, J. Membrane Biol. **208**, 193 (2005).
[159] N. Kuerka, J. Pencer, J. N. Sachs, J. F. Nagle, and J. Katsaras, Langmuir **23**, 1292 (2007).
[160] G. Bldt, H. Gally, A. seelig, J. Seelig, and G. Zaccai, Nature **271**, 182 (1978).
[161] G. Bldt, H. Gally, J. Seelig, and G. Zaccai, Journal of Molecular Biology **134**, 673 (1979).
[162] L. Herbette, C. Napolitano, and R. McDaniel, Biophysical Journal **46**, 677 (1984).
[163] N. Kuerka, J. F. Nagle, J. N. Sachs, S. E. Feller, J. Pencer, A. Jackson, and J. Katsaras, Biophysical Journal **95**, 2356 (2008).
[164] V. F. Sears, Neutron News **3**, 26 (1992).
[165] R. W. Benz, F. Castro-Romn, D. J. Tobias, and S. H. White, Biophysical Journal **88**, 805 (2005).
[166] D. T. Cromer and J. B. Mann, Acta Crystallographica Section A **24**, 321 (1968), ISSN 1600-5724, URL http://dx.doi.org/10.1107/S0567739468000550.
[167] A. Braun, E. Brandt, O. Edholm, J. Nagle, and J. Sachs, Biophysical Journal **100**, 2112 (2011).
[168] J. Pan, T. T. Mills, S. Tristram-Nagle, and J. F. Nagle, Phys. Rev. Lett. **100**, 198103 (2008).
[169] A. Hodzic, M. Rappolt, H. Amenitsch, P. Laggner, and G. Pabst, Biophysical Journal **94**, 3935 (2008).
[170] N. Kucerka, J. F. Nagle, J. N. Sachs, S. E. Feller, J. Pencer, A. Jackson, and J. Katsaras, Biophys. J. **95**, 2356 (2008), ISSN 0006-3495, URL http://www.sciencedirect.com/science/article/B94RW-4VB4SVM-S/2/7ede236c4e83d16a6fe57cc3b1894349.
[171] J. Pan, S. Tristram-Nagle, and J. F. Nagle, Phys. Rev. E **80**, 021931 (2009).
[172] G. Khelashvili, G. Pabst, and D. Harries, The Journal of Physical Chemistry B **114**, 7524 (2010).
[173] F. Heberle, J. Pan, R. Standaert, P. Drazba, N. Kuerka, and J. Katsaras, European Biophysics Journal **41**, 875 (2012), ISSN 0175-7571.
[174] J. C. Fogarty, M. Arjunwadkar, S. A. Pandit, and J. Pan, Biochimica et Biophysica Acta (BBA) - Biomembranes **1848**, 662 (2015).
[175] J. N. Sachs, H. I. Petrache, and T. B. Woolf, Chemistry and Physics of Lipids **126**, 211 (2003).
[176] J. B. Klauda, N. Kuerka, B. R. Brooks, R. W. Pastor, and J. F. Nagle, Biophysical Journal **90**, 2796 (2006).
[177] N. Kuerka, J. D. Perlmutter, J. Pan, S. Tristram-Nagle, J. Katsaras, and J. N. Sachs, Biophysical Journal **95**, 2792 (2008).
[178] A. R. Braun, J. N. Sachs, and J. F. Nagle, The Journal of Physical Chemistry B **117**, 5065 (2013).
[179] S. K. Hansen, K. Bertelsen, B. Paaske, N. C. Nielsen, and T. Vosegaard, Progress in Nuclear Magnetic Resonance Spectroscopy **8889**, 48 (2015).
[180] A. Spaar and T. Salditt, Biophys J **85**, 1576 (2003), ISSN 0006-3495.
[181] R. B. Best and J. Mittal, Proteins: Structure, Function, and Bioinformatics **79**, 1318 (2011), ISSN 1097-0134, URL http://dx.doi.org/10.1002/prot.22972.
[182] K. A. Beauchamp, Y.-S. Lin, R. Das, and V. S. Pande, Journal of Chemical Theory and Computation **8**, 1409 (2012).
[183] S. Rauscher, V. Gapsys, M. J. Gajda, M. Zweckstetter, B. L. de Groot, and H. Grubmller, Journal of Chemical Theory and Computation **11**, 5513 (2015).

ToDo

P.